Chinese Journal of
POLYMER SCIENCE

REVIEW

https://doi.org/10.1007/s10118-024-3112-x
Chinese J. Polym. Sci. **2024**, *42*, 693–710

Recent Advances in Asymmetric Structural Composites for Excellent Electromagnetic Interference Shielding: A Review

Ying Zhou[a,c], Bai Xue[a,b,c], Lan Xie[a,b,c*], Chang-Mei Wu[a], and Qiang Zheng[d*]

[a] *Department of Polymer Materials and Engineering, College of Materials and Metallurgy, Guizhou University, Guiyang 550025, China*
[b] *State Key Laboratory of Public Big Data, Guizhou University, Guiyang 550025, China*
[c] *National Engineering Research Center for Compounding and Modification of Polymer Materials; National and Local Joint Engineering Research Center for Functional Polymer Membrane Materials and Membrane Processes, Guiyang 550014, China*
[d] *Department of Polymer Science and Engineering, Zhejiang University, Hangzhou 310027, China*

Abstract Since electromagnetic pollution is detrimental to human health and the environment, numerous efforts have been successively made to achieve excellent electromagnetic interference shielding effectiveness (EMI SE) *via* designing the hierarchical structures for electromagnetic interference (EMI) shielding polymer composites. Among the plentiful structures, the asymmetric structures are currently a hot spot, principally categorizing into multi-layered, porous, fibrous, and segregated asymmetric structures, which endows the high EMI shielding performance for polymer composites incorporated with magnetic, conductive, and/or dielectric micro/nano-fillers, due to the "absorption-reflection-reabsorption" shielding mechanism. Therefore, this review provides the retrospection and summary of the efforts with respect to abundant asymmetric structures and multifunctional micro/nano-fillers for enhancing EMI shielding properties, which is conducive to the booming development of polymeric EMI shielding materials for the promising prospect in modern electronics and 5-generation (5G) technology.

Keywords Asymmetric structure; Micro/nano functional filler; Polymer composite; Electromagnetic interference shielding

Citation: Zhou, Y.; Xue, B.; Xie, L.; Wu, C. M.; Zheng, Q. Recent advances in asymmetric structural composites for excellent electromagnetic interference shielding: a review. *Chinese J. Polym. Sci.* **2024**, *42*, 693–710.

1 INTRODUCTION

With the rapid growth of modern electronic equipment and circuit technology, electromagnetic waves (EMWs) as the transmission medium inevitably cause severe electromagnetic pollution which will not only hazard human health but also interfere with precision instruments.[1] In order to reduce electromagnetic radiation pollution, numerous efforts have been successively put into the design strategy and shielding mechanism for exploiting high-efficiency electromagnetic interference (EMI) shielding composites. Preparing high-performance EMI shielding composites requires meticulous consideration of interface interactions, rational structural design, and material selection. Metals, such as copper,[2] aluminum,[3] silver,[4] and stainless steel,[5] have frequently been utilized as EMI shielding materials due to their high dielectric constants and electrical conductivity. However, the inherent disadvantages of metal-based materials (*e.g.*, processing difficulty and high density) restrict their practical application in advanced electronic devices.[6]

In recent years, conductive polymer composites (CPCs)[7,8] have assumed an important role in the development of EMI shielding composites due to their corrosion resistance, flexibility, lightweight, and processability.[9] A series of functional micro/nanofillers including two dimensional (2D) transition metal carbides/nitrides ($Ti_3C_2T_x$ MXene),[10] reduced graphene oxide (rGO),[11,12] carbon nanotubes (CNTs),[13,14] boron nitride nanosheets (BNNS),[15] and carborundum (SiC),[16] black phosphorus (BP),[17] and liquid metal (LM),[18] have been introduced into the polymer matrix to endow the excellent EMI shielding performance.[19] BP and LM acted as new conduc-

* Corresponding authors, E-mail: mm.lanxie@gzu.edu.cn (L.X.)
E-mail: zhengqiang@zju.edu.cn (Q.Z.)

Received December 18, 2023; Accepted February 27, 2024; Published online April 10, 2024

tive fillers and have become a research hotspot to fabricate EMI shielding composite due to their high conductivity. An ultra-thin MXene-based composite film (20 μm) containing BP and nickel (Ni) chains (M-B-M(Ni)) with integrated highly efficient EMW shielding. The assembled BP converted EMW's energy into heat in the visible band. MXene-Galinstan liquid metal hybrid yields superior electrical conductivity and exhibits a shielding effectiveness of 66.3 dB. Due to the incorporation of Galinstan particles in between the conductive layers of the MXene, these MXene composite films exhibited excellent EMI shielding performance because the liquid metal formed an efficient conduction path between the MXene interlayers and significantly reduced the interlayer resistance. Besides, the fluidity of the liquid metal enhanced the adhesion between the MXene layers through a bridging effect which assured high electrical conductivity over a long range of fabricated composite films. To improve EMI SE by enhancing multi-layered reflective interfaces, most studies have focused on sandwich structures and symmetric alternating multilayer structures.[20] In addition, the reflective interfaces of EMI shielding materials can also be significantly improved by micropore structures, which lengthens the propagation path and leads to the enhancement of re-reflection and scattering of EMWs in the porous materials. Unfortunately, a large number of conductive fillers are demanded to reach the satisfactory electromagnetic interference shielding effectiveness (EMI SE) of CPCs due to the commonly nonconductive and nonmagnetic polymer matrix, leading to the deteriorative mechanical properties and serious secondary electromagnetic radiation pollution.

Interestingly, the incorporation of carbon nanomaterials and magnetic nanofillers increases the dielectric loss and thus improves the absorption of microwaves.[21,22] In the case of micro/nanostructures,[23,24] the main shielding mechanism for EMI shielding based on CPC[25,26] may change from the conventional reflection mechanism to a multiple reflection or absorption-dominate mechanism.[27] When the incident surface is designed as an impedance-matching absorbing plane, EMWs can easily enter the internal EMI shields with little reflection. A part of the incoming EMWs is absorbed and/or consumed into heat in the EMI shields. If the other surface is assembled as an impedance-mismatching reflecting plane, a majority of the remaining EMWs can be reflected back inside and further reabsorbed and/or dissipated in the form of heat. Hence, the asymmetric structures consisting of impedance-matching absorbing and impedance-mismatching reflecting layers are beneficial for the attenuation of EMWs and the reducing reflection, which can greatly relieve the secondary electromagnetic radiation contamination. In the asymmetric structures, magnetic nanoparticles, such as iron, cobalt, nickel, ferrous metal oxides, and their carbon hybrids, are commonly filled in the impedance-matching (low electrical conductivity) layer, which leads to the descended reflection and increased absorption of EMWs due to dielectric and magnetic losses. Most of the conductive fillers, such as silver nanowires (AgNWs), copper nanowires (CuNWs), MXene, CNTs, rGO, Ag nanoparticles ($AgNP_S$),[28] nanogold ($AuNP_S$),[29] and so on, are usually introduced into the impedance-mismatching (high electrical conductivity) layer, which can greatly reflect EMWs into the inside of the shielding materials owing to the large impedance mismatch. AgNWs, CuNWs, Ag nanoparticles and nanogold could decrease the energy of EMWs through ohmic loss. At the same time, the microstructure of the nano-conductive filler can prolong the reflection path and significant effect on the multiple-directional internal reflection of the EMWs. The conductive networks constructed by the nano-conductive filler made the interface contact, which can produce more and more free charge spontaneous accumulation to enhance the polarization relaxation loss.

In the related research reports, the asymmetric structure that is divided into four main categories (multilayered, fibrous, porous, and segregated asymmetric structures) is receiving much attention in the development of EMI shielding materials (Fig. 1). Herein, the shielding mechanism and the latest research progress of polymer-based EMI shielding composites with asymmetric structures were summarized. Moreover, the micro/nano-fillers compounded in the EMI shielding composites with asymmetric structures are also described. Depending on the reasonable layout of the impedance-matching layer and reflecting layer, the polymeric composites with asymmetric structures exhibit excellent EMI shielding efficiency by reason of the "absorption-reflection-reabsorption" shielding mechanism. Finally, the research trends and challenges of EMI shielding materials with asymmetric structures are prospected. This review helps to construct the structure-performance relationship of EMI shielding composites with asymmetric structures and guides EMI shielding material selection and design.

Fig. 1 The category of different fillers and structures of EMI shielding composites with asymmetric structures.

2 SHIELDING MECHANISM OF EMI SHIELDING COMPOSITES WITH ASYMMETRIC STRUCTURES

Electromagnetic radiation from outside can damage electronic systems by inducing false voltages and currents.[30] Therefore, to protect electronic systems, a shield must be created to block electromagnetic radiation emitted by computer circuits, electric motors, cell phones, and other devices. EMWs through the

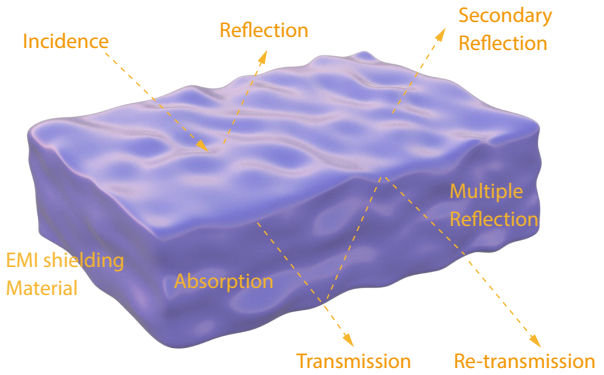

Fig. 2 Schematic diagram of the interaction between EMWs and shield.

shield mainly include four types: transmission, absorption, multiple reflection and reflection, on the basis of the plane-wave electromagnetic transmission line theory of Schelkunoff (Fig. 2).

The total EMI SE (SE_T) is defined as the logarithmic ratio of the incident EMW power (P_o), electric field (E_o), and magnetic field (H_o) to the transmitted EMW power (P_t), electric field (E_t), and magnetic field (H_t), respectively.[31]

$$SE_T\,(dB) = 10\log\frac{P_o}{P_t} = 20\log\frac{E_o}{E_t} = 20\log\frac{H_o}{H_t} \quad (1)$$

Attenuation through reflection (SE_R), absorption (SE_A), and multiple reflections (SE_M) together constitute SE_T. The equation is expressed as follows:

$$SE_T\,(dB) = SE_R + SE_A + SE_M \quad (2)$$

SE_R arises from the difference in surface impedance of two-propagating media. Thus, SE_R is directly correlated to the electrical conductivity of materials, according to Eq. (3):

$$SE_R\,(dB) = 168 + 10\log\frac{\sigma_r}{\mu_r f} \quad (3)$$

where σ_r represents the electrical conductivity of the shield, μ_r is the magnetic permeability of the shield, and f denotes the frequency of the signal source.

As shown in Eq. (4), SE_A is enhanced with the increasing electrical conductivity and magnetic permeability of the shield.

$$SE_A\,(dB) = 8.68t\left(\sqrt{\frac{\sigma_r\omega\mu_r}{2}}\right) = 8.68\frac{t}{\delta} \quad (4)$$

where t is the thickness, ω is the angular frequency which is equal to $2\pi f$, and δ is the skin depth which is defined as the distance at which the electric field intensity drops to $1/e$ of the original incident wave value. The skin depth (δ) can be calculated by Eq. (5):

$$\delta = \frac{1}{\sqrt{\pi f\sigma_r\mu_r}} \quad (5)$$

The multiple reflections between the front and back of the shield promote SE_T, which can be expressed as:

$$SE_M\,(dB) = 20\log(1 - e^{-\frac{2t}{\delta}}) \quad (6)$$

When SE_T exceeds 15 dB or t approaches/exceeds the skin depth, SE_M becomes negligible. When SE_A exceeds 10 dB, SE_M can also be disregarded.[32]

CPCs with an asymmetric structure are composed of an absorptive layer and a reflective layer, contributing to the EMI shielding mechanism of "absorption-reflection-reabsorption". The loss of EMWs in the absorptive layer (impedance matching layer) mainly originates from absorption loss, which is divided into dielectric loss and magnetic loss. Dielectric loss (δ_d) depends on the complex permittivity, which is constituted of real (ε') and imaginary (ε'') permittivity ($\tan\delta_d = \varepsilon''/\varepsilon'$), where ε' stands for the energy storage capacity, but ε'' represents the energy dissipation power.[33] Dielectric loss mainly includes conduction loss which is the energy loss caused by the current flows across the medium in the course of conductance, and polarization loss which is categorized as ionic polarization, electric dipole polarization and interfacial polarization.[34] In addition, magnetic loss such as eddy current loss, dimensional resonance loss, *etc*. is largely influenced by the magnetic permeability ($\mu = \mu' - j\mu''$), where μ' and μ'' are also real and imaginary permeability, respectively.[35]

After EMWs are absorbed in the impedance-matching layer, the residual EMWs reach the reflective layer (impedance-mismatching layer). Due to the large impedance mismatch between reflective and absorptive layers, a majority of the remaining EMWs are reflected back to the absorptive layer. The interaction between EMWs and the free-charge carriers determines the reflection of EMWs. Multiple reflections in the shielding materials with asymmetric structures can prolong the propagation path and enhance the dissipation of EMWs. Moreover, the reflected EMWs are reabsorbed in the impedance matching layer *via* dielectric loss and magnetic loss, which finally causes the high EMI shielding performances.

3 CHARACTERIZATION METHODS

The study of the electromagnetic properties of materials is usually carried out in a wide frequency band, so sweep frequency measurement is required. Sweep frequency measurement technology is generally developed based on a vector network analyzer (VNA). VNA can measure EMI SE by recording the variation of power or intensity of EMWs after passing across the shielding materials. Transmission lines, shielded boxes, and shielded rooms are composed of VNA to investigate complex signals, response amplitude, and phase of different signals. The transmission line method, for example, the coaxial transmission line approach and the waveguide method, has been developed into the most popular technique.[36] EMI SE is calculated by the acquired complex scattering parameters (S parameters), S_{11} (or S_{22}), and S_{12} (or S_{21}). Total EMI SE (SET), absorption (SE_A), reflection (SE_R), power coefficient of transmission (T), absorption (A), and reflection (R) could be calculated detailedly by the following equations:

$$T = |S_{12}|^2 = |S_{21}|^2 \quad (7)$$

$$R = |S_{11}|^2 = |S_{22}|^2 \quad (8)$$

$$A = 1 - R - T \quad (9)$$

$$SE_T = 10\lg\left(\frac{1}{|S_{12}|^2}\right) = 10\lg\left(\frac{1}{|S_{21}|^2}\right) = 10\lg\left(\frac{1}{T}\right) \quad (10)$$

$$SE_R = 10\lg\left(\frac{1}{1-|S_{11}|^2}\right) = 10\lg\left(\frac{1}{1-|S_{22}|^2}\right) = 10\lg\left(\frac{1}{1-R}\right) \quad (11)$$

$$SE_A = 10\lg\left(\frac{1-|S_{11}|^2}{|S_{12}|^2}\right) = 10\lg\left(\frac{1-|S_{22}|^2}{|S_{21}|^2}\right) \quad (12)$$

4 RESEARCH PROGRESS OF EMI SHIELDING COMPOSITES WITH ASYMMETRIC STRUCTURES

Generally, the structures of the EMI shielding materials have a great effect on the shielding properties. It is worth noticing that a variety of polymer-based EMI shielding composites with asymmetric structures have been widely investigated and exploited. This section introduces polymer-based EMI shielding composites with asymmetric structures, comprising multi-layered structures, fibrous structures, porous structures and segregated structures. And the functional fillers incorporated into these composites are also discussed.

4.1 Asymmetric Films

At present, the multi-layered film structures have drawn widespread concern by virtue of easily integrating the superiority of individual constituents and achieving super-universal properties. The multi-layered structures are facilely constructed by vacuum filtration, volatile forming, hot-pressing and substrate-assisted methods. In comparison with the common symmetric multi-layered structures (including sandwich structure),[37,38] asymmetric multi-layered structures feature the difference in structure, filler, and/or conductivity between the front and back sides, offering feasible advantages in EMI shielding. The asymmetric multi-layered structures exhibit the tailorable electrical conductivity of the incident surface and reflective surface, which provides the "weak reflection-absorption-strong reflection-reabsorption" shielding mechanism and thus greatly improves EMI SE.[30] The EMI shielding properties of asymmetric multi-layered composite films filled with functional CNTs, rGO, MXene, and metal-organic frameworks (MOFs) are summarized in Table 1.

4.1.1 Carbon nanotubes (CNTs)

CNTs have been widely applied to fabricate EMI shielding composites due to their high conductivity and large aspect ratio.[51] However, the disadvantage of adding CNTs into the polymer is that CNTs are easy to agglomerate in a polymer matrix, resulting in a decrease in the electrical conductivity and mechanical properties of the composite.[52,53] Therefore, some scholars are committed to promoting the dispersion of CNTs in polymer matrix by compounding with magnetic nanoparticles or other conductive materials, which is beneficial for constructing three-dimensional (3D) asymmetric conductive networks and obtaining prominent EMI shielding properties.[54]

He *et al*. prepared an asymmetric membrane by suction-filtrating polyaniline-coated carbon nanotubes (CNTs@PANi) and poly(vinyl pyrrolidone)-coated Fe_3O_4 nanorods (Fe_3O_4@PVP) under a magnetic field.[39] The CNTs@PANi/Fe_3O_4 membrane is composed of a vertically aligned top region and a weakly aligned bottom region, illustrating the typical asymmetric structures of benefit for the EMI shielding (Figs. 3a–3c). The asymmetric CNTs@PANi/Fe_3O_4 membrane exhibits SE_T of 49.3 dB and pretty heat dissipation at a thickness of 270 μm and density of 0.74 kg/dm^3. A value is increased to 0.81 at the EMW incident from the top surface, while it is only 0.45 at the incident direction from the bottom surface. The vertically aligned CNTs in the top region reduce the electrical conductivity and impedance mismatching, thus the top region has a strong absorption capacity for EMWs. However, the plane CNTs in the bottom region construct conductive networks and play a role as an efficient reflective band.

The recent publication of He and coworkers showed that multilayered antimony trioxide-nickel-carbon nanotubes/polydimethylsiloxane (Sb_2O_3-Ni-MWCNTs/PDMS) composites with asymmetric or symmetric structures were fabricated by using PDMS as matrix and Sb_2O_3-Ni-MWCNTs as multiple fillers *via* layer-by-layer curing method.[55] Predictably, the electric-magnetic-dielectric synergism largely enhanced the EMI shielding performance of multilayered Sb_2O_3-Ni-MWCNTs/PDMS composites (Figs. 3d–3f). The asymmetric MWCNTs-Sb_2O_3-Ni/M composites constituted of 1.6MWCNTs-1.2Sb_2O_3-1.2Ni/PDMS and 4.0MWCNTs/PDMS layers exhibit a high EMI SE_T of 55.7 dB and pretty A of 0.80. The outstanding EMI shielding performance of Sb_2O_3-Ni-MWCNTs/PDMS composite is attributable to the Salisbury screen effect which occurs in layered-structure composites and the synergistic effect of electric-magnetic-dielectric losses.

Table 1 Asymmetric composite films with multi-layered structures for EMI shielding applications.

Author(s)	Composites	EMI SE (dB)	Ref.
Wenjun He *et al*. (2022)	CNT@polyaniline (PANi)/Fe_3O_4	50.00	[39]
Qingwei Tao *et al*. (2022)	Fe_3O_4-polydimethylsiloxane (PDMS)/CNT/Cu	75.10	[40]
Guirong Hu *et al*. (2022)	Cellulose nanofiber (CNF)/rGO@Fe_3O_4&CNF/AgNWs	112.90	[41]
Yadong Xu *et al*. (2018)	rGO@Fe_3O_4/tetra needle-like zinc oxide whisker (T-ZnO)/silver (Ag)/waterborne polyurethane (WPU)	87.20	[42]
An Sheng *et al*. (2020)	Fe_3O_4@rGO/multi-walled carbon nanotubes (MWCNT)/WPU	35.90	[43]
Bing Zhou *et al*. (2022)	CNF/MXene/AgNW	55.90	[44]
Fudong Zhang *et al*. (2022)	MXene-AgNWs/cellulose	61.90	[45]
Zhengzheng Guo et al. (2022)	Cobalt ferrite ($CoFe_2O_4$) @MXene-AgNWs/cellulose	73.30	[46]
Wentao Cao *et al*. (2019)	CNTs/MXene/cellulose	38.40	[47]
Zhiqiang Lai *et al*. (2023)	Polyurethane (PU)/AgNW/Cu/Ni	90.00	[48]
Mushan Yuan *et al*. (2022)	Carbonized zeolitic imidazolate frameworks (C-ZIF67)/graphene nanoplates (GNP)/cellulose	50.50	[49]
Tian Mai *et al*. (2023)	Carbonized zeolitic imidazolate frameworks (CZIF)/MXene/nanocellulose	62.40	[50]

https://doi.org/10.1007/s10118-024-3112-x

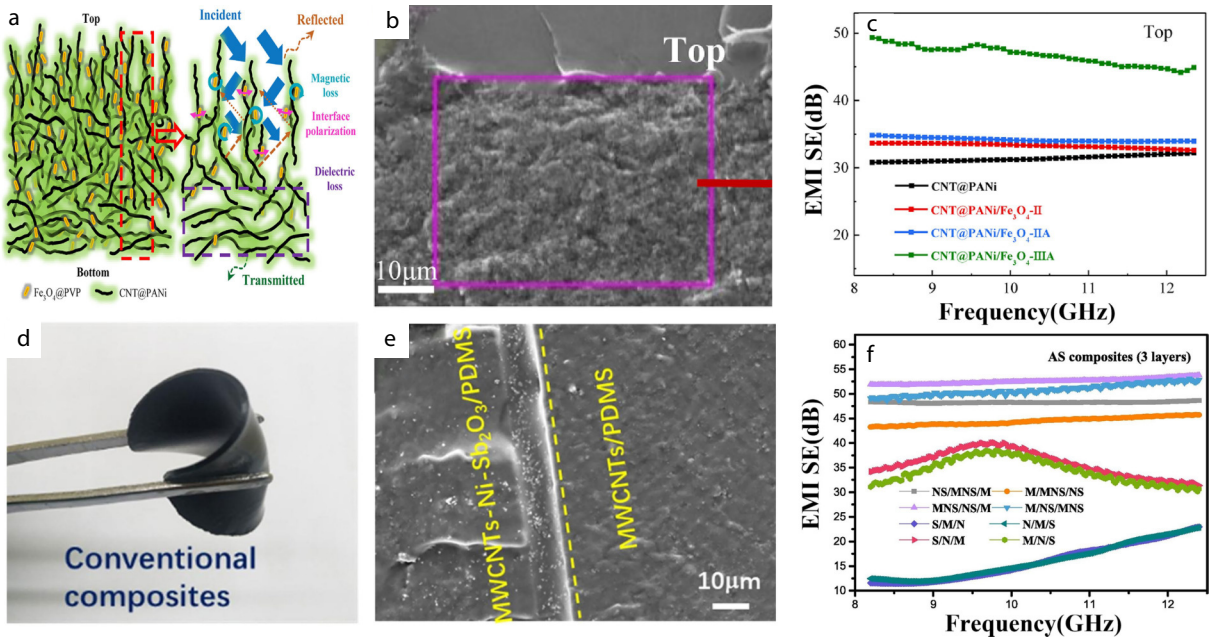

Fig. 3 (a) EMI shielding mechanism, (b) SEM image, and (c) EMI SE of asymmetric CNTs@PANi/Fe_3O_4 composite films. (Reproduced with permission from Ref. [39]; Copyright (2022), Elsevier); (d) Digital photo, (e) SEM image, and (f) EMI SE of Sb_2O_3-Ni-MWCNTs/PDMS composites. (Reproduced with permission from Ref. [55]; Copyright (2022), Elsevier.)

Tao and coworkers successfully fabricated the Fe_3O_4-PDMS/CNT/Cu membranes with step-wised asymmetric structures.[40] Fe_3O_4-PDMS was coated on the CNT paper, and Cu was deposited on the other side *via* electron beam evaporation. The asymmetric Fe_3O_4-PDMS/CNT/Cu membrane exhibits a high EMI SE_T of 75.1 dB with a thickness of about 0.3 mm. The top Fe_3O_4-PDMS layer and middle compact CNT layer result in magnetic loss, electrical loss and multiple reflections, respectively. Finally, Cu as a highly reflective layer located at the bottom of the membrane reflects more EMWs back to CNT and Fe_3O_4-PDMS layers. Thus, the Fe_3O_4-PDMS, CNT and Cu synergistically contribute to obtaining the amazing EMI shielding ability.

4.1.2 Reduced graphene oxide (rGO)

The rGO possesses extraordinary properties, such as tensile strength,[56] electrical conductivity,[57] high surface area, and aspect ratio,[58] which are conducive to the construction of a conductive network in composites and the enhancement of EMI shielding properties. Furthermore, the comprehensive properties of rGO-filled composites are largely affected by the dispersion, size, and inter-sheet connections in the matrix.[59] Similar to CNTs, rGO has been modified to improve its dispersion ability and electrical property for building a highly conductive network in the matrix, and further improving the EMI shielding performance.[60,61]

Recently, Hu and coworkers prepared a cellulose nanofiber/reduced graphene oxide@Fe_3O_4&cellulose nanofiber/silver nanowires (CNF/rGO@Fe_3O_4&CNF/AgNWs) composite film with an asymmetric structure that shows an EMI SE_T of 112.9 dB and satisfactory mechanical properties at a thickness of 0.067 mm.[41] In this work, the CNF/rGO@Fe_3O_4 layers were designed as the negative gradient absorbing layers, and the CNF/AgNWs layers form the positive gradient reflective layers (Figs. 4a–4c). Reasonable arrangement of the absorbing layer and reflecting layer leads EMWs to experience a decreasing absorption and increasing reflection process in the asymmetric composite film. Moreover, the prominent EMI shielding property can be achieved by the magneto-electric synergy of AgNWs and rGO@Fe_3O_4 and the reasonable structure layout.

Xu and coworkers prepared the asymmetric gradient membranes which were composed of solution-mixing WPU, T-ZnO/Ag and rGO@Fe_3O_4.[42] Because of different densities of fillers leading to different deposition rates, T-ZnO/Ag is deposited on the bottom but rGO@Fe_3O_4 is located at the top of the membrane. The composite membrane reveals an EMI SE_T of 87.2 dB and a low A-value of 0.61 at a thickness of 500 μm, which illustrates the strong absorption ability. rGO@Fe_3O_4 located at the top of the membrane reduces the impedance mismatching, presenting low reflection characteristics. Moreover, T-ZnO/Ag with a dense network deposited at the bottom of the membrane plays a role as an efficient reflective layer, which greatly improves the EMI shielding performances.

An *et al.* exploited electromagnetic gradient membranes with an EMI SE_T of 35.9 dB and R-value of 0.27, which presented low reflection characteristics.[43] Fe_3O_4@rGO/MWCNT/WPU membranes are constituted of one MWCNT/WPU layer at the bottom and three Fe_3O_4@rGO/WPU layers with gradient rGO content in Fe_3O_4@rGO at the upper part (Figs. 4d–4f). The A value constantly increases with an enhancement of MWCNT concentration, meanwhile, tanδ_d significantly enhances with an increase of gradient. This phenomenon can be explained by the fact that the enhanced MWCNT concentration leads to a more compact conductive network in the reflection layer which improves conduction loss and causes more EMWs to reflect back to the absorption layer. Moreover, more free charges accumulating at the layer interface with the increasing gradient trigger more microscopic dipole moments and

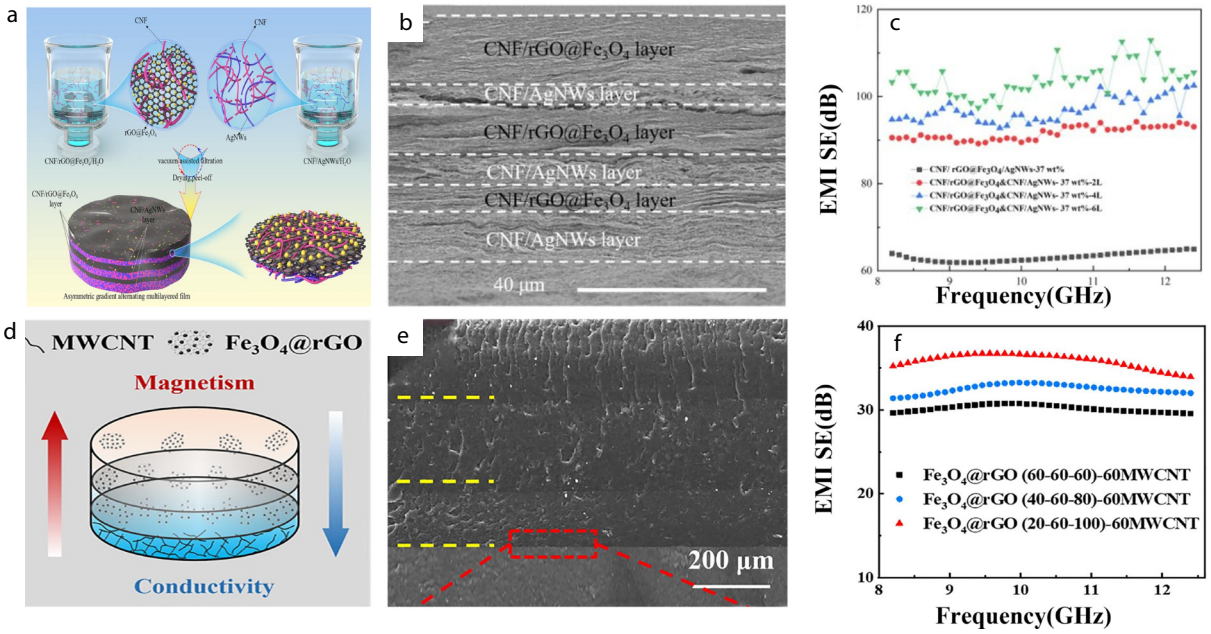

Fig. 4 (a) Filtration diagram, (b) SEM image, and (c) EMI SE of CNF/rGO@Fe_3O_4&CNF/AgNWs films. (Reproduced with permission from Ref. [41]; Copyright (2022), Elsevier); (d) Digital photo, (e) SEM image, and (f) EMI SE of Fe_3O_4@rGO/MWCNT/WPU composites. (Reproduced with permission from Ref. [43]; Copyright (2020), Elsevier.)

thus improve the interfacial polarization. Therefore, Fe_3O_4@rGO/MWCNT/WPU composites with larger gradients present satisfactory EMI SE and extremely low reflection characteristics.

4.1.3 MXene

MXene as an emerging material possesses high electrical conductivity, which has been widely applied in EMI shielding composites.[62] A lot of charge carriers on the MXene surface result in EMW reflection due to the impedance mismatch between MXene and air.[63] The interaction between the free charge carriers and EMWs evokes current and dipole, causing ohmic and polarization losses, respectively.[64] MXene nanosheets can form stable dispersions in water and some polar organic solvents,[65] so solution processing techniques have become the most commonly employed methodologies.[66] Thus, a variety of processing strategies, such as vacuum filtration,[67] dip coating,[68] spray coating,[69] spin coating,[70] and interfacial assembly,[71] can be utilized to prepare MXene/polymer composites with multi-layer structures.[72]

Cao *et al*. fabricated the flexible CNTs/MXene/CNF (CMC) membranes with gradient sandwich structures *via* an alternately filtrating method.[47] The gradient and sandwich CMC composite film is composed of CM-5 (5 mg of MXene and 1 mg of CNT), CNF (4 mg), CM-10 (10 mg of MXene and 1 mg of CNT), CNF (4 mg), and CM-15 (15 mg of MXene and 1 mg of CNT) layers, which displays a superb EMI SE of 38.4 dB with a mere thickness of 38 μm. It is concluded that the gradient structure is crucial to the proportion of SE_A and SE_R, instead of SE_T. Nonetheless, the sandwich structure can largely enhance the EMI shielding performances in comparison with the homogeneous structure, due to the increased interlayered multiple reflection and interfacial polarization. Moreover, the CMC film with gradient and sandwich structure holds fascinating mechanical performances with respect to tensile strength of 97.9 MPa and toughness of 2.1 MJ/m^3.

Zhou *et al*. fabricated asymmetric sandwich CNF/MXene/AgNWs membranes with a favorable EMI SE_T of 55.9 dB *via* step-by-step vacuum-assisted filtration.[44] CNF is designed as the external layers to protect the internal conductive layers, and the MXene and AgNWs layers are situated in the middle of the CNF/MXene/AgNWs membranes. Notably, the *R*-value of CNF/MXene/AgNWs membranes is higher than 0.9, indicating the reflection-dominated shielding mechanism. In addition, the conductive networks formed by the synergistic MXene and AgNWs largely accelerate the electron conduction and impart outstanding EMI SE shielding ability for the CNF/MXene/AgNWs composite membranes.

Coincidentally, another asymmetric CNF/MXene/AgNWs membrane with low AgNWs and MXene content was also prepared by Zhang *et al*. *via* a vacuum filtration method.[45] CNF/MXene and CNF/AgNWs are architected as the top and bottom layers, and CNF is formed as the middle layer. The asymmetric CNF/MXene/AgNWs membrane displays a superior EMI SE of 61.9 dB (Figs. 5a–5c), due to "zigzag" reflection mechanisms and multiple reflection effects. The structural variation can give rise to the magnifying SE_A and SE_R by increasing the dielectric loss and impedance mismatch, respectively. In contrast with uniform membrane, the resultant asymmetric multilayered membrane also reveals superior mechanical properties, such as tensile strength of 137 MPa and fractured strain of 5.7%.

Guo *et al*. fabricated an asymmetric $CoFe_2O_4$@MXene-AgNWs/CNF membrane with a double-layered structure by a two-step vacuum-assisted filtration. The asymmetric membrane comprising $CoFe_2O_4$@MXene/CNF layer with low conductivity and AgNWs/CNF layer with high conductivity exhibits an excellent EMI shielding effectiveness of 73.3 dB at a thickness of 100 μm (Figs. 5d–5f).[46] The $CoFe_2O_4$@MXene/

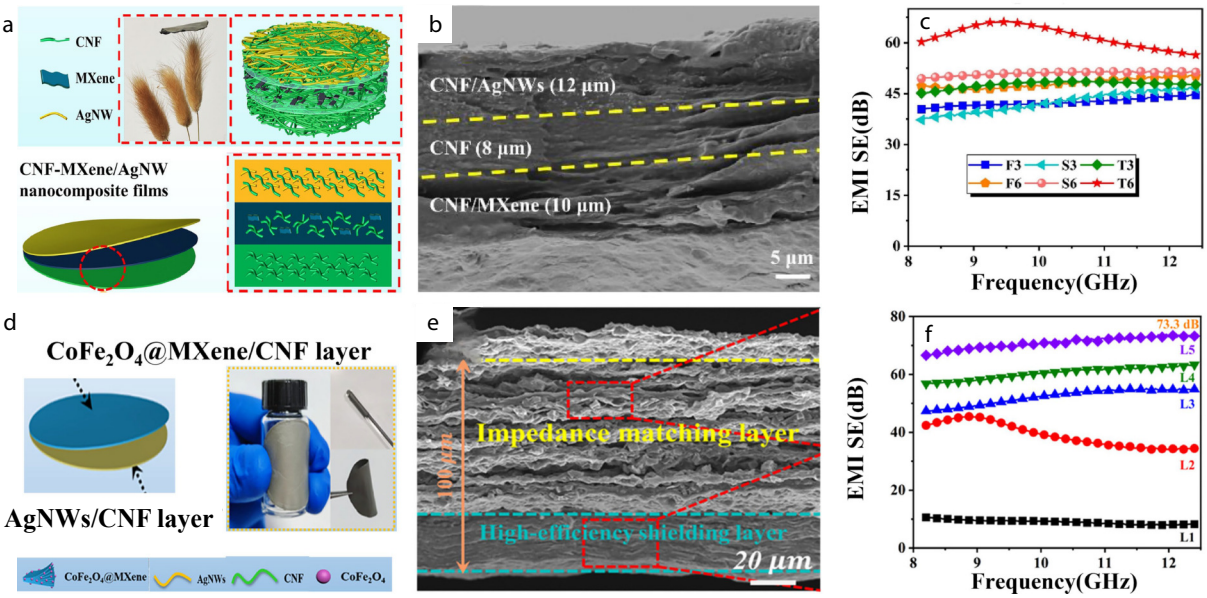

Fig. 5 (a) Digital photo, (b) SEM image, and (c) EMI SE of CNF-MXene/AgNWs membranes. (Reproduced with permission from Ref. [45]; Copyright (2022), Elsevier); (d) Digital photo, (e) SEM image, and (f) EMI SE of $CoFe_2O_4$@MXene/CNF films. (Reproduced with permission from Ref. [46]; Copyright (2022), American Chemical Society.)

CNF layer as the impedance matching layer reduces surface reflections and enhances magnetic and dielectric losses. Meanwhile, the highly conductive AgNWs/CNF layer acts as the impedance mismatching layer to increase the reflection. Arising from the synergistic effect of $CoFe_2O_4$, MXene and AgNWs, and the reasonable arrangement of absorptive and reflective layers, the asymmetric membrane can achieve efficient EMI SE at a low thickness. In addition, the heterogeneous interface leads to space charge distribution at the heterogeneous interface, which can further attenuate EMWs by dipole polarization.

Carbonyl irons (CI) is a widely utilized functional filler due to its high magnetic permeability, high saturation magnetization strength, excellent wave absorption properties, and wide absorption band. Liu *et al.* fabricated the asymmetric CI/$Ti_3C_2T_x$/polyvinylidene fluoride (PVDF) membranes *via* magnetic-field-induced and subsequent hot pressing methods.[73] Adding 20 wt% CI and 10 wt% $Ti_3C_2T_x$, the asymmetric membrane illustrates a maximum EMI SE_T value of 42.8 dB at a thickness of 400 μm. The multilayered CI-rich layers promote the transformation of the shielding mechanism from reflection to absorption, due to the largely enhanced multiple reflections and magneto-electric synergistic effect of CI-$Ti_3C_2T_x$. Furthermore, the asymmetric multilayered composites exhibit the superior EMI SE to the homogeneous and traditionally alternate/sandwich layered composites.

4.1.4 Metal-organic frameworks (MOFs)

MOFs are new porous materials with the great virtues of large surface area, high porosity, regular topology, and interconnected channels. They are constructed by the inorganic metal centers and bridge-linked organic ligands through self-assembly. Meanwhile, the metal frame enhances the impedance matching between material and air and offers a mass of active sites for scattering and attenuating EMWs, which increases EMW absorption.[74,75] After pyrolysis, carbon-MOF materials can preserve pretty porous structures and highly specific surfaces, which has sparked wide research attention in the area of alleviating electromagnetic pollution.

Yuan *et al*. fabricated the porous carbonized zeolitic imidazolate frameworks (C-ZIF67)/graphene nanoplates (GNP)/cellulose membranes *via* vacuum-assisted filtration and hot-pressing methods, which comprises asymmetric bilayer structures (low conductive C-ZIF67 layer and highly conductive GNP layer) (Figs. 6a–6c).[49] The asymmetric membrane corresponds to a high *A* value of 0.87 with an outstanding EMI SE of 50.5 dB. In particular, the porous structure of C-ZIF67 facilitates the suppression of eddy current effects and the promotion of multi-interface polarization, leading to the effective dissipation and absorption of EMWs. Thus, the asymmetric structure composed of porous C-ZIF67 and dense GNP exhibits an "absorption-reflection-reabsorption" multiple losses shielding principle, which ensures the dominant role of absorption.

Mai *et al*. fabricated absorption-dominated EMI shielding carbonized zeolitic imidazolate frameworks (CZIF)/MXene/CNF (CZMN) films *via* vacuum-assisted filtration.[50] In the CZMN films with an asymmetric bilayer structure, magnetic CZIF/CNF with low conductivity works as an adsorption layer and highly conductive MXene plays a role as a reflective layer. When EMWs are incident from the CZIF/CNF layer, the absorption rate SE_A/SE_T of CZMN films all remains higher than 70%, owing to the synergy between magnetic loss of CZIF and scattering loss of TOCNF, meanwhile, an optimal EMI SE of 62.4 dB is achieved for CZMN-3 film. Besides, the EMI SE_T of bilayers CZMN films is greatly raised with the increasing MXene content, while SE_A/SE_T can retain little fluctuation. Thus, the absorption-dominated EMI shielding CZNN films can efficiently reduce secondary electromagnetic pollution, overcoming the excessive reflection drawback of common MXene composites.

https://doi.org/10.1007/s10118-024-3112-x

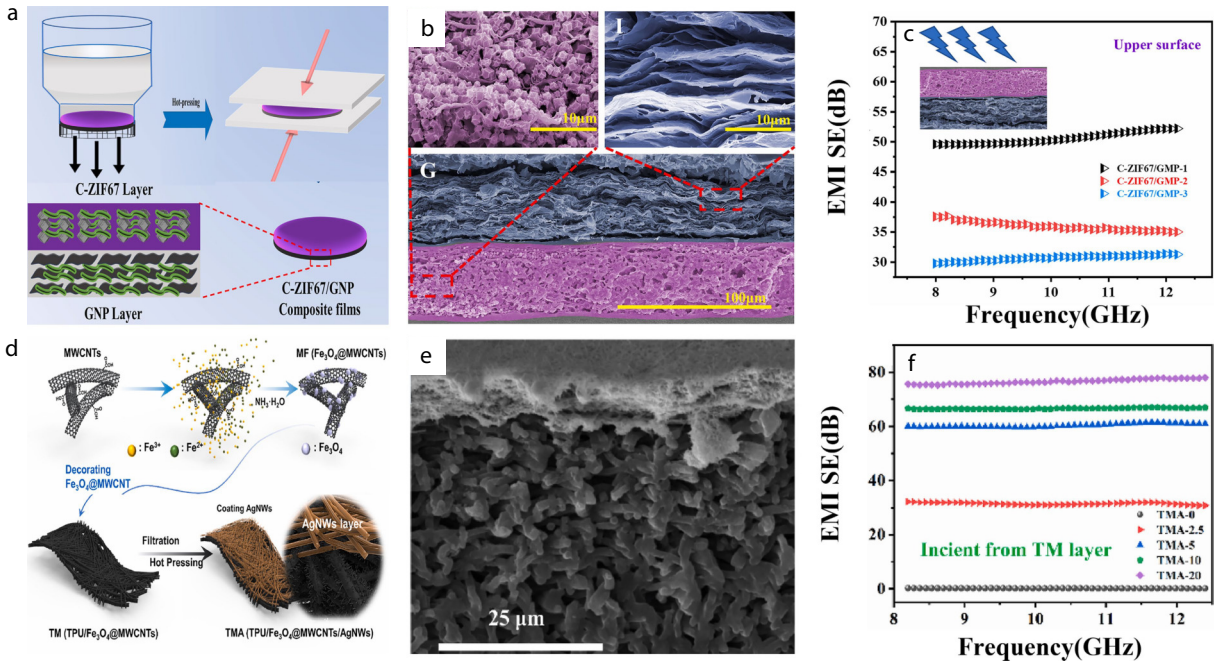

Fig. 6 (a) Fabrication schematic, (b) SEM images, and (c) EMI SE of C-ZIF67/GNP/cellulose films. (Reproduced with permission from Ref. [49]; Copyright (2022), Elsevier); (d) Schematic diagram of electrostatic spinning, (e) SEM image, and (f) EMI SE of TPU/Fe_3O_4@MWCNTs/AgNWs films. (Reproduced with permission from Ref. [76]; Copyright (2023), Elsevier.)

In summary, the requirements of thin thickness and high EMI SE can be achieved by the design of asymmetric composites with multi-layered structures. The multilayered structures integrating different functional compositions can easily obtain the synergistic effect of electro-dielectric-magnetic losses, which is greatly conducive to the EMI SE. In addition, the rational arrangement of various layers can lead to excellent multiple reflections and adjustable EMW absorption/reflection, which is of great significance for the practical application of asymmetric multilayered EMI shields. Currently and in the future, asymmetric multilayered structures are designed and constructed for the preparation of prominent EMI shielding materials to create a high-performance EMI shielding strategy.

4.2 Asymmetric Fabrics

Flexible conductive fabrics have attracted a lot of attention due to their significant potential in weaponry, wearable electronics and biomedicine.[77] The current methods for preparing fabrics include the weave method, hydrothermal method, electrostatic spinning method, *etc*. Generally, fabrics are beneficial for the regulation of the distribution of nanofillers to build stable 3D conductive networks.[78] Various conductive nanofillers, such as MXene,[79] MWCNTs,[80] Ag nanoparticles,[81] Ag nanowires[82] and graphene,[83] are added into fabrics using vacuum filtration, *in situ* growth, spraying, dip-coating, or other methods to prepare the excellent EMI shielding fabrics.[84] However, conductive fabrics have defects of insufficient EMI shielding, poor durability and high reflectivity. Hence, it is of significance to construct nano-micro structures in conductive fabrics to achieve desirable and adjustable EMI shielding properties.[85] Particularly, asymmetric EMI shielding fabrics are introduced in the following section.

Zhang and his colleagues prepared asymmetric thermoplastic polyurethane (TPU)/MWCNT@Fe_3O_4/AgNWs fibrous films (TMA) by a series of electrospinning, dip-coating, filtration, and hot-pressing processes. The special asymmetric fibrous structures built in TMA possess TPU/MWCNT@Fe_3O_4 (TM) layers at the sublayer for EMW absorption and AgNWs layer at the top for EMI shielding and thermal conduction. The TMA film at 20 mg of AgNWs content shows excellent EMI shielding up to 78.48 dB with *R*-value as low as 0.56 and the preeminent thermal conductivity of 7.83 W/mK (Figs. 6d–6f).[76] Without respect to the incident direction from the TM layer or AgNWs layer, EMI SE_T has little difference but SE_A and SE_R are drastically changed. When EMWs are incident from the TM layer, lower reflection occurs due to the decreasing impedance mismatching, and MWCNT@Fe_3O_4 in TMs prompts the EMW absorption through dielectric loss and magnetic loss. Afterward, the entered EMWs are largely reflected and re-attenuated by the upper AgNWs layer before transiting through the whole fibrous film.

Lv and coworkers prepared poly(vinyl alcohol) (PVA)/liquid metal (LM)/boron nitride (BNNS)/silk fibroin (SF) membranes with gradient structure through electrospinning and mold pressing.[86] Due to the gradient structure and increasing PVA/LM content, the PVA/LM/BNNS/SF membranes reach the highest EMI SE of 75 dB in the X-band and a large *R*-value of 0.951, which demonstrates a reflection-dominated shielding mechanism of PVA/LM/BNNS/SF composite. Ohmic loss between LM particles and interfacial polarization loss at the interface of LM with PVA can convert EMW energy into heat in the top PVA/LM layer. Then a majority of EMWs are reflected at the interface between the top and middle layers, due to the high impedance mismatching accompanied by the LM continuous conductive pathway. Moreover, multiple reflections between the top PVA/LM layer and the middle LM layer

further dissipate or absorb EMWs.

Li and coworkers designed a flexible gradient composite consisting of negative PVDF@GO gradient and positive AgNWs gradient *via* the reverse dip-coating method, which featured high shielding capability and low reflection properties.[87] The EMI SE_T of the Cotton/AgNWs/PVDF@GO composite reaches 50 dB with a rather low R of 0.39 due to the synergistic effect of GO and AgNWs and the double gradient structures. Finally, the negative PVDF@GO gradient and positive AgNWs gradient endow the pretty hydrophobicity, wonderful EMI shielding capacity, and low reflection of EMWs.

Xiao *et al*. prepared flexible double-layered polyurethane (PU)/Ag/Fe_3O_4 (PANM) fabrics with an asymmetric structure via an electrospinning process.[88] AgNPs/PU nanofibers (bottom reflective layer) with shell-core structure were fabricated by plating AgNPs on the prefabricated PU nanofibers *via* hydrazine hydrate reduction. Then Fe_3O_4/PU nanofibers were directly electro-spun onto the AgNPs/PU as the top absorption layer. At last, the interface of the lower AgNPs/PU and upper Fe_3O_4/PU layers was fused *via* the photothermal treatment. The asymmetric PANM fabrics display satisfactory mechanical properties and an outstanding EMI SE of 69.6 dB with an *R*-value of 0.79. The strong interfacial interactions between the two function layers ensure the tensile property and surface stability. The absorption-reflection-reabsorption shielding mechanism in asymmetric PANM fibrous films causes more dissipation of the EMWs and wonderful EMI SE.

Zhang *et al*. fabricated double-layer fiber-based aramid fibers (AF)@Ni/Cu/Fe_3O_4/WPU composite with metal microtube conductive networks *via* casting methods.[89] WPU dispersions containing magnetic particles are casted on the framework of metallized nonwoven fabrics which forms asymmetric conductive and magnetic multilayer structure. The asymmetric WPU-based composite fabrics exhibits a high EMI SE value of 55.8 dB in the X-band. Additionally, the Fe_3O_4 particles settled due to gravity, aiding in the absorption of EMWs. The composite film forms a magnetic multilayer and an asymmetrical conductive structure, obtaining an EMI SE value of 55.8 dB. The metallized AF@Ni/Cu nonwoven fabric has magnetic particles laminated on the frame, and these magnetic particles enhance the absorption of EMWs. The exceptional properties of strong absorption and low reflection point to a shielding mechanism that is absorption-oriented.

Illuminated by muscle-like nanostructure, Chen *et al*. developed the spandex fiber textiles/AgNPs/AgNWs/MXene/iron cobalt-carbon (FeCo-C) (Ag_DMC) textiles *via* a sequence of dip-coating methods.[90] The flexible Ag_DMC textiles comprise the AgNPs layer, AgNWs layer, MXene layer, and FeCo-C layer from interior to exterior, corresponding to the conductivity from high to low. Tightly packed functional nanoparticles are similar to connective tissues, endowing Ag_DMC textiles with the outstanding EMI SE of 88 dB with a low *R*-value of 0.168 as well as sensing and heat generating ability. AgNWs are dip-coated on the AgNPs layer to construct the high reflective layer, which works as "endomysium". Moreover, FeCo-C nanoparticles stemming from ZIF-67 are electrostatically adsorbed on the MXene layer to form the absorbing layer. Furthermore, the $Ag_DM_1C_2$ sample in the condition of deformation at stretch 75% still remains 49.7 dB EMI SE_T, which demonstrates the excellent EMI shielding performances of this Ag_DMC textiles even under high deformation. The progressive conductivity design strategy for the Ag_DMC textiles and the synergic effect of magnetic-electric-dielectric losses contribute to the high absorption and dissipation of EMW energy. In addition, Ag_DMC textiles correspond to the superb stability and reliability of EMI shielding on complicated conditions, and high sensitivity and rapid response for strain sensors.

In summary, fabrics prepared using electrostatic spinning, weave, *etc*., provide attachment points for the functionalized fillers and form a continuous and complete conductive network. 3D conductive networks in the conductive fabrics promote electronic conduction and EMWs attenuation. The fabrics with asymmetric conductive networks exhibit superior flexibility, tensile strength, and adjustable EMI shielding properties, which has set the stage for making their mark in EMI shielding fields.

4.3 Asymmetric Foams

The 3D porous EMI shielding composites possess the advantages of lightweight, high mechanical strength and excellent absorbing properties, making them suitable for the reduction of secondary pollution. The preparation methods of porous composites can be divided into phase separation, template method, supercritical carbon dioxide foaming method, and so forth. The distribution of fillers in the polymer matrix can affect the density, diameter of the pore and electrical conductivity. The porous structures can improve the impedance-matching characteristics between the shield and air to some extent, due to the presence of gas in the vesicles. Furthermore, multiple reflections of EMWs in pores extend the propagation path, thus enhancing the dissipation ability of the porous material. However, the exorbitant size of the pore will generally cause leakage of EMWs and reduce the EMI shielding performance. As can be seen from the designing strategy of asymmetric foams, the back reflection layer in asymmetric foams can efficiently reduce the escape of EMWs. Table 2 summarizes the EMI shielding performance of asymmetric porous composites.

4.3.1 CNTs

Xue *et al*. prepared step-wise asymmetric Ni-coated melamine foam (Ni@MF)/CNT/polybutylene adipate terephthalate (PBAT) EMI shielding composites *via* electroless plating, vacuum-assisted self-assembly and solution encapsulation processes.[91] The asymmetric composite is designed with a loose Ni@MF layer and a compact CNT layer to successfully realize the directional EMI shielding function. When the EMWs are incident from the Ni@MF layer and CNT layer, EMI SE_T values of the asymmetric composites are 38.3 and 29.5 dB, respectively. The rational arrangement of asymmetric structures triggers the "weak reflection-absorption-strong reflection-reabsorption" shielding principle, at the incident direction from the Ni@MF layer. On the contrary, asymmetric Ni@MF/CNT/PBAT composites exhibit a "strong reflection-absorption" mechanism when EMWs are incident from the CNT layer. As a result, Ni@MF/CNT/PBAT composites with step-wise asymmetric structures achieve novel directional EMI shielding properties and may provide a new investigation window for material science.

Zhang *et al*. fabricated the flexible asymmetric Ni@CNTs/CNTs/PDMS composites *via* selective electroplating

https://doi.org/10.1007/s10118-024-3112-x

Table 2 EMI SE of asymmetric porous composites.

Author(s)	Composition	EMI SE (dB)	Ref.
Bai Xue *et al*. (2022)	Ni@MF/CNT/PBAT	38.30	[91]
Jiapeng Zhang *et al*. (2022)	Ni@CNTS/CNTS/PDMS	70.00	[92]
Jianming Yang *et al*. (2020)	SR/Ag@HGMs/Fe_3O_4@MWCNTs	59.39	[93]
Jianming Yang *et al*. (2021)	VMQ/Ag@GF/MWCNT/Fe_3O_4	78.60	[94]
Zuomin Lei *et al*. (2021)	AgFD/CNT/TPU	88.50	[95]
Hongji Duan *et al*. (2020)	EBAg/FeCo@rGO/WPU	90.00	[96]
Qiang Gao *et al*. (2022)	a-EP/f-RGO/Ni-chains	40.82	[97]
Mengyao Li *et al*. (2023)	MF/Pani/Fe_3O_4@rGO/AgP/PDMS	70.00	[98]
Guangde Liu *et al*. (2022)	TiO_2-$Ti_3C_2T_x$/rGO/PDMS	58.00	[99]
Tongcheng Zuo *et al*. (2023)	MXene/CNT/Fe_3O_4/WPU	20.06	[100]

and encapsulation methods.[92] The adjustable conductivity and permeability ensure the composites achieve an EMI SE_T of 70 dB and an average SE_R as low as 3.1 dB. Through selective electroplating, the electromagnetic Ni@CNTs layer and the electrically conductive CNTs layer form asymmetric structures. Moreover, Ni@CNTs/CNTs were encapsulated by PDMS to obtain Ni@CNTs/CNTs/PDMS with satisfying mechanical properties. When EMWs are incident from the Ni@CNTs side, more EMWs will pass into the inside of Ni@CNTs/CNTs/PDMS composites due to the superb impedance matching. Magnetic hysteresis loss, eddy current loss, and multiple reflection loss contribute to greatly dissipating EMWs inside the composites. The remanent EMWs reaching the high conductive CNT layer will be reflected back due to the impedance mismatch between Ni@CNTs and CNTs. Regardless of the EMWs incident from the CNTs side or the Ni/CNTs side, the EMI SE_T of Ni@CNTs/CNTs/PDMS remains almost unchanged, but SE_R shows considerable variation of as much as 5.3 dB.

Yang *et al*. obtained the asymmetric silicone rubber (SR)/Ag@hollow glass microspheres (Ag@HGMs)/Fe_3O_4@MWCNTs composite (SAHFM) foams through solution mixing and $scCO_2$ foaming (Figs. 7a–7c).[93] The composite foam with an asymmetric gradient structure exhibits an outstanding EMI SE value of 59.39 dB with a thickness of 700 μm. Due to a large density difference between the Ag@HGMs and Fe_3O_4@MWCNTs, Ag@HGMs are floated on the upper surface of composites, constructing a highly conductive layer, and Fe_3O_4@MWCNTs nanoparticles are deposited at the bottom of composites, forming a carbon-magnetic absorption layer. In addition, smaller pores of HGMs are gathered at the top and larger pores generated by $scCO_2$ foaming are distributed in the middle of SAHFM foams, constructing the gradient cellular structures. A large number of magnetic particles and bubbles accumulate on one side of this gradient composite foam, effectively reducing the impedance mismatch as well as improving the magnetic loss and dielectric loss. The selective distribution of functional fillers supplies a novel thought into the design of asymmetric EMI shielding foams.

Yang and his colleagues prepared heterogeneous silicone rubber (VMQ)/Ag@GF/MWCNT/Fe_3O_4 composite foams with

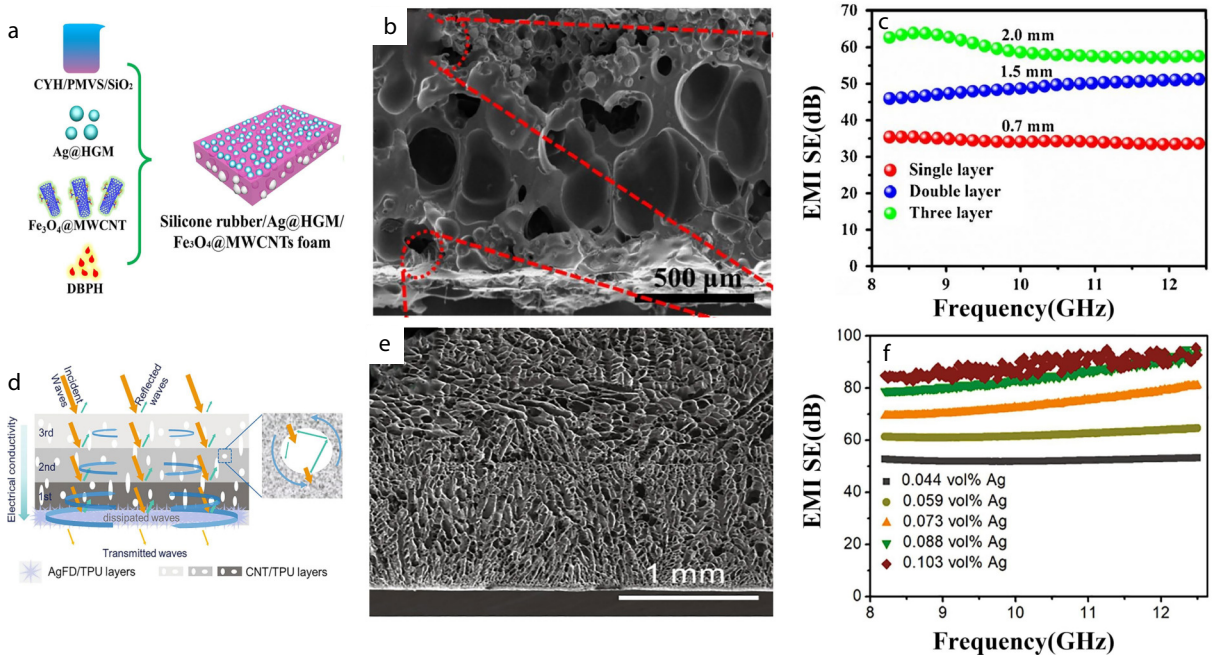

Fig. 7 (a) SAHFM foam, (b) SEM image, and (c) EMI SE of SAHFM foam. (Reproduced with permission from Ref. [93]; Copyright (2020), Elsevier); (d) Electromagnetic shielding mechanism, (e) SEM image, and (f) EMI SE of AgFD/CNT/TPU composite foam. (Reproduced with permission from Ref. [95]; Copyright (2021), Elsevier.)

gradient porous structure *via* layer-by-layer combination and supercritical carbon dioxide ($scCO_2$) foaming.[94] The heterogeneous foam displays a high average EMI SE of 78.6 dB and A value of 0.82, which certificates the absorption-dominant electromagnetic shielding mechanism. From bottom to top, the positive gradient structure (AgM3M2M1F20) consists of the Ag@GF layer, MWCNT (3.0 wt%) layer, MWCNT (2.0 wt%) layer, MWCNT (1.0 wt%) layer, and Fe_3O_4 (20 wt%) layer. Analogously, the negative gradient structure (AgM1M2M3F20) exhibits the increasing MWCNT content (M1M2M3) from bottom to top. The largest pores are distributed in the MWCNT (1.0 wt%) layer and the minimum pores are located in the MWCNT (3.0 wt%) layer, due to the different viscosity restricting the growth of pores during the foaming process. It is worth noting that the *A*-value of the positive gradient structure is remarkably higher than that of the negative gradient structure, which shows that the positive gradient structure possesses strong absorption properties of EMWs. The F20 layer displays low conductivity and good impedance matching, which makes more incident EMWs reach the internal of the foam. Due to the increasing conductivity of the positive gradient structure, the interface polarization and dielectric loss are increasing. Meanwhile, the multilayer porous structure leads to the enhancement of the dissipation of EMWs because of the multiple reflections at the cellular interface. Besides, the plane Ag@GF in the bottom region constructs conductive networks and plays a role as an efficient reflective band.

Silver fractal dendrites (AgFD) have superior electrical, optical and catalytic properties, compared to traditional silver particles. Lei and coworkers prepared asymmetric AgFD/CNT/TPU composite foams by layer-by-layer construction and freeze-drying methods (Figs. 7d–7f).[95] The asymmetric foam possesses an outstanding EMI SE_T of 88.5 dB and an *A*-value exceeding 0.9 at a thickness of 3.4 mm. The bottom reflective AgFD layer and the upper gradient absorptive CNT/TPU layer compose the asymmetric structures, which provides a novel design insight for preparing absorption-dominated EMI shielding composites. The gradient porous structure of the CNT/TPU layer reduces the impedance mismatching and thus reflection as well as provides dielectric loss and relaxation loss against EMWs. AgFD/TPU layers owning high conductivity can reflect the transmissive EMWs back to the CNT/TPU layer. Notably, the gradient porous structures of the AgFD/CNT/TPU composites will raise multiple reflections and thus internal absorption of EMWs.

4.3.2 rGO

Duan and coworkers fabricated the asymmetric Ag-coated expanded polymer bead/graphene-supported iron-cobalt/waterborne polyurethane (EBAg/FeCo@rGO/WPU) composite foams *via* the directional freeze-drying and density-induced filler separating methods.[96] The asymmetric structure is composed of the deposited FeCo@rGO magnetic nanoparticles at the sedimentary as an impedance-matching layer and EBAg particles at the upper surface as a conductive layer. FeCo@rGO layer with high permeability supplies strong absorption due to dielectric and hysteresis loss. On the other side, the EBAg layer with large conductivity provides intensive reflection owing to the great impedance mismatching. Moreover, the poriferous structure causes multi-interface absorption, which enhances the absorption of the EMWs in composite foams. The directional pores provide a favorable channel parallel to the EMW direction, further reducing the reflection of EMWs. Thus, these asymmetric composite foams obtained a high EMI SE_T of 84.8 dB and *A* of 0.92.

Gao *et al*. prepared asymmetric epoxy resin (a-EP)/functionalized reduced graphene oxide (f-rGO)/Ni-chains foams *via* thermal compressing and supercritical carbon dioxide ($scCO_2$) foaming.[97] Prospectively, the asymmetric a-EP/f-rGO/Ni-chains foams exhibit an EMI SE_T of 40.82 dB in the X-band. In the asymmetric composites, a-EP/Ni-chain at the positive surface acts as the absorptive layer, and a-EP/f-rGO at the negative surface works as the reflective layer. Hence, the discrepancy of the *R*-value achieves 0.5, when EMWs are incident from positive and negative surfaces of the asymmetric foams. EMWs transmitting inside a-EP/f-rGO/Ni-chains foams are dissipated through polarization loss, ohmic loss, magnetic loss, and multiple internal reflections derived from f-rGO, Ni-chains and cell structures. Eventually, a-EP/f-rGO/Ni-chains foams can convert the shielding mechanism from reflection to absorption (*i.e.*, absorption-reflection-reabsorption) *via* the rational layout of asymmetric structures.

Li *et al*. produced asymmetric melamine foam/polyaniline/Fe_3O_4@reduced graphene oxide/Ag-plated aramid paper/polydimethylsiloxane (MF/PANI/ Fe_3O_4@rGO/AgP/PDMS) composites *via in situ* polymerization, dip-coating and electroless plating.[98] Arising from the magnetoelectric synergy of Fe_3O_4@rGO and conductive PANI, the asymmetric composites exhibit a high EMI SE_T of 70 dB and an outstanding A value of 0.86. When the incident wave enters the upper porous MF/PANI/Fe_3O_4@rGO layer, a relatively low reflection is reached due to the excellent impedance matching between the lowly conductive MF/PANI/Fe_3O_4@rGO layer and air. In addition, the porous structures cause the interior multiple reflections, extending the transmitting path of EMWs and attenuating EMW energy. The dense conductive AgP paper adhered on the other side largely reflects EMWs back to the MF/PANI/Fe_3O_4@rGO layer, which is resubjected to the absorption in the porous magnetic layer.

Liu and coworkers prepared asymmetric gradient porous titanium dioxide-$Ti_3C_2T_x$ (TiO_2-$Ti_3C_2T_x$)/rGO frameworks *via* 3D printing, freeze-drying and annealing treatment.[99] Then, gradient porous TiO_2-$Ti_3C_2T_x$/rGO/PDMS composites were fabricated *via* vacuum-impregnating PDMS into TiO_2-$Ti_3C_2T_x$/rGO frameworks. The gradient structure is presented with the gradually tapering aperture from the top larger aperture to the bottom smaller aperture. The gradient composite with square aperture features an EMI SE_T of 58 dB at a thickness of 0.2 cm, owing to the synergistic effect of conductive loss, dipole polarization and multiple-reflection derived from 3D printed structures. It is worth noting that the EMI SE of TiO_2-$Ti_3C_2T_x$/rGO/PDMS composite with a gradient pore structure is much higher than that of the uniform porous composites, due to the adjustable impedance matching and enhanced internal multiple reflections.

4.3.3 MXene

Zuo *et al*. fabricated CNT/Fe_3O_4/WPU aerogel *via* vacuum freeze-drying method.[100] Afterward, MXene nanosheets were infiltrated at the bottom of CNT/Fe_3O_4/WPU aerogel to obtain the asymmetric MXene/CNT/Fe_3O_4/WPU aerogel. According to the

progressive modular design principle, CNT/Fe_3O_4/WPU and MXene/WPU are designed as the impedance matching layer and the reflective layer, respectively. The asymmetric MXene/CNT/Fe_3O_4/WPU aerogel shows a SE_T of 20.06 dB and a low *R* of 0.396 as the amount of MXene was only 2.35 vol%, which certifies the absorption-based shielding mechanism. These encouraging results are derived from the asymmetric porous structures of MXene/CNT/Fe_3O_4/WPU aerogel, which improves the surficial impedance matching and the internal multiple reflections. Besides, multiple heterojunctions in MXene/CNT/Fe_3O_4/WPU aerogel will generate interface polarization and dissipation of EMWs. Therefore, the construction of asymmetric structures combining CNTs with MXene is an effective approach to acquiring absorption-dominated EMI shielding.

Pei and coworkers manufactured directional EMI shielding rGO@Fe_3O_4 (rGF)/ rGO@MXene (rGM)/PDMS composites with asymmetric structures using dual-needle 3D printing.[101] The asymmetric structure consists of the conductive rGM layer and the magnetic rGF layer. EMI SE_T of the rGF/rGM/PDMS composites reaches 30.79 and 38.75 dB, when EMWs are incident from the rGM layer and rGF layer, respectively, exhibiting the SE difference (ΔSE) as much as 8 dB for different incident directions. *R*-value is reduced from 0.87 to 0.48, when EMWs are incident from the rGF layer, demonstrating the absorption-dominated shielding mechanism converted from the reflection-dominated one. The design strategy of the combination of porous magnetic and dense conductive layers can produce a special "weak reflection-absorption-strong reflection-reabsorption" course for the incident EMWs.

Yao *et al*. prepared a series of asymmetric MXene/aramid nanofibers (ANF)/polyimides (PI) (AMAP) aerogels *via* vacuum-assisted filtration combined with freeze-casting.[102] The asymmetric aerogel gives an average EMI SE_T of 47.8 dB with a low *R*-value of 0.0138 and a satisfied IR stealth property. The tight ANF/MXene layer as an enhanced reflective layer is deftly combined with the porous MXene/ANF/PI aerogel through a unidirectional freezing method, which achieves a surprisingly low reflection characteristic. The discontinuous MXene nanosheets existing in MXene/ANF/PI aerogels generate local conduction loss and polarization loss, which leads to large absorption of EMWs in AMAP. The residual EMWs will reach the dense MXene layer and be reflected back immediately due to the impedance mismatch. The EMWs reflected back to the MXene/ANF/PI aerogel can be reabsorbed and additionally attenuated by the destructive interference.

Zuo *et al*. fabricated asymmetric MXene/WPU/Melamine (MF) foams and MXene/Ag@ZnO/WPU/Melamine (MAF) foams using WPU and melamine foams as agglomerate and skeleton, respectively, *via* unidirectional evaporation in combination with a vacuum-drying method.[103] The asymmetric MAF foam presents an outstanding EMI SE_T of 39.9 dB and a low *R*-value of 0.1423. The conductivity of the composite foam gradually decreases from the sides to the middle, effectively regulating the reflection characteristics. Meanwhile, the electrical conductivity at the top of MAF foams is obviously lower than that at the bottom, because both MXene and Ag@ZnO are deposited at the bottom due to the larger density. When EMWs are incident from the top, a majority of EMWs enter the MAF foams with relatively low reflection, due to the decreased impedance mismatching. Noticeably, the highly conductive bottom of MAF foams can efficiently prevent the escape of the EMWs. What's more, gravity-induced separation is an effective method for constructing asymmetric structures in preparing highly efficient EMI shielding materials.

In the future, researchers should pay more attention to subtly adjusting and designing the asymmetric micro-nano porous structures. The design strategy of the porous absorptive layer combined with the compact reflective layer will be utilized to develop more EMI shielding materials with absorption-dominated characteristics to make full use of their unique advantages.

4.4 Asymmetric Segregated Composites

Polymer composites with segregated structures have received a lot of attention due to their low filler content and high EMI performance.[104] The segregated structure of conductive nanofillers concentrated around the polymer matrix particles rather than randomly dispersed in the polymer matrix makes it easier to form conductive pathways at the polymer particle interfaces.[105,106] In other words, constructing segregated structures in polymers with the same content of conductive fillers results in a higher conductivity of polymer composites than that of randomly distributed structures.[107,108] Similar to the porous structure, the segregated structures have a large number of conductive interfaces formed by the conductive networks. EMWs are reflected many times and attenuated by the dielectric loss when they are transmitted to the conductive interface. There are commonly three methods to prepare asymmetric EMI shielding composites with segregated structures, including solid mechanical mixing, freeze-drying of emulsion, and selective dispersion of conductive fillers. This section mainly discusses asymmetric EMI shielding composites with segregated structures based on specific design strategies.

Sun and coworkers fabricated asymmetrically segregated TPU/CNT/Ag composites comprised of a segregated TPU/CNT layer and a conductive Ag layer *via* thermal cladding, vacuum-assisted hot compression and blade-coating methods.[109] When CNTs are clustered together at the interface of TPU particles, a CNT conductive path in the TPU/CNT layer is constructed. Based on the above design strategy, the segregated TPU/CNT/Ag composites showed a high EMI SE of 79.4 dB and an *R*-value of 0.54 (Figs. 8d–8f). Through electrical loss, dielectric loss, and multiple reflections, the penetrated EMWs are dissipated and absorbed by the TPU/CNT composite layer. The residual EMWs reaching the Ag layer will be largely reflected and attenuated by the high conductive layer. In addition, the reflected EMWs are reabsorbed by the segregated TPU/CNT layer, which leads to the high-absorption EMI shielding capacity.

Asymmetric silver nanowire/iron-nickel oxide/expanded polymer microsphere (AgNWs/$NiFe_2O_4$/EPM) composites with segregated structures were prepared by combining an AgNWs/EPM layer and a $NiFe_2O_4$/EPM layer *via* layer-by-layer filtration and hot pressing.[110] The asymmetric composites feature an outstanding EMI SE_T of 72.5 dB and a low *R*-value of 0.15. In the absorbing and reflecting layers, EPMs are respectively surrounded by $NiFe_2O_4$ and AgNWs to assemble segregated networks. Interestingly, the EMI SE_T of the asymmetric segregated composite foam is much higher than that

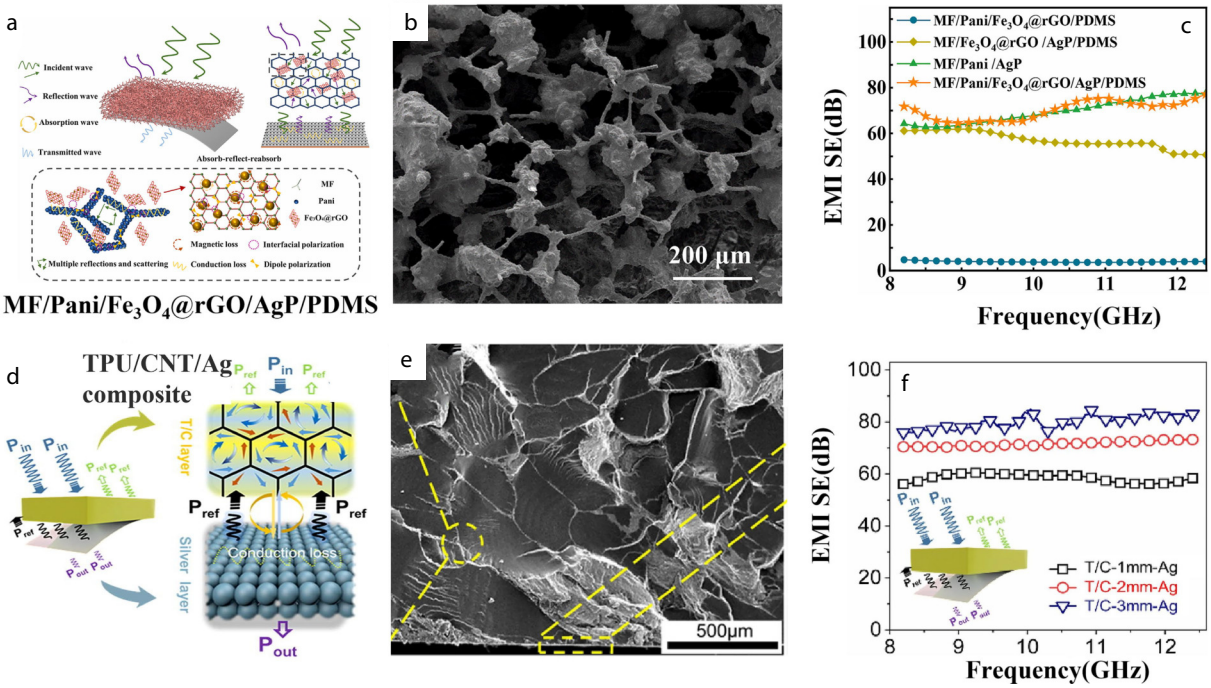

Fig. 8 (a) Electromagnetic shielding mechanism, (b) SEM image, and (c) EMI SE of MF/Pani/Fe_3O_4@rGO/AgP/PDMS foam. (Reproduced with permission from Ref. [98]; Copyright (2023), Elsevier); (d) Electromagnetic shielding mechanism, (e) SEM image, and (f) EMI SE of TPU/CNT/Ag composite foam. (Reproduced with permission from Ref. [109]; Copyright (2021), Elsevier.)

of a homogeneous foam, which shows that the asymmetric structure with conductive segregated networks allows the localized gathering of the filler and thus better-shielding properties. $NiFe_2O_4$/EPM layer owns impedance matching between air and composites, which ensures more EMWs enter into the interior of the composites. The incoming EMWs are attenuated by the magnetic loss, dielectric loss, and interfacial polarization loss in the $NiFe_2O_4$/EPM layer. Due to the impedance mismatch, EMWs reaching the AgNWs/EPM layer are reflected into the $NiFe_2O_4$/EPM layer and are then dissipated again.

Wang *et al*. prepared asymmetric Ag@CNTs/polystyrene (PS) microbeads (Ag@CPMs)/CNTs/WPU composite foams with segregated structures *via* vacuum filtration and freeze-drying.[111] The asymmetric segregated composite foam presents a high EMI SE_T of 42.4 dB, a low *R*-value of 0.16, and satisfactory mechanical properties. The porous CNTs/WPU aerogel layer works as an upper absorbed layer with the regulatable impedance matching. Meanwhile, the Ag@CPMs layer consisting of a 3D stacked Ag shell and CNTs/PS core with a compact segregated structure acts as the bottom reflective layer. The rational arrangement of asymmetric structure is vital to the outstanding EMI shielding performances of Ag@CPMs/CNTs/WPU foams. The incident EMWs from porous CNTs/WPU aerogel with appropriate impedance matching will be dissipated by the multiple refractions, dielectric loss, and eddy current loss. When the EMWs reach the Ag@CPMs layer, a lot of EMWs will be reflected back to the CNTs/WPU aerogel and reabsorbed by multiple reflections. Moreover, the residual EMWs are dissipated by the conducive loss and polarization loss between the CNTs/PS core and the Ag shell.

Wu and coworkers prepared nickel@silicon carbide (Ni@SiCw)/graphene nanosheet (GNP)/PVDF EMI shielding composites by solution mixing and hot pressing, which shows an EMI SE of 36.83 dB.[112] Silicon carbide has the advantages of high resistance and good performance in absorbing electromagnetic waves. Dielectric properties of Ni@SiCw are significantly enhanced compared with silicon carbide. A rational design of Ni@SiCw in the absorber layer could provide impedance matching while offering effective EMW absorption efficiency. Distributing GNP in the reflector layer can provide the composite with better EMI SE and reduce the escape of EMWs. The asymmetric structure of the Ni@SiCw layer and the GNP layer makes the microwave undergoes an absorption-reflection-reabsorption process. In addition, the composite shows an absorption-dominated shielding mechanism when the EMWs are incident from the Ni@SiCw surface and a reflection-dominated shielding mechanism when incident from the GNP surface.

In conclusion, the segregated structure can better constrain the conductive filler to form a conductive framework, which reduces the loading amount of filler.[113] The segregated structure demonstrates distinctive SMI SE_T and scalable functionality that will not let you down.

5 CONCLUSIONS AND OUTLOOK

According to this review, the latest progress of asymmetric EMI shielding composites with excellent comprehensive properties focusing on multi-layered, fibrous, porous, and segregated structures has been discussed in detail. Various research groups have presented new research achievements on the design and fabrication of EMI shielding composites with asymmetric structures. On the basis of these recent advances, we summarized

certain conclusions and development tendencies of the asymmetric EMI shielding materials as follows.

(1) Asymmetric EMI shielding composites with multilayered structures can meet the requirements of low thickness and high EMI SE_T, which is especially suitable for the application of miniaturized electronics. The EMI shielding properties of asymmetric multilayered composites can be effectively adjusted by the category, distribution, and content of functional fillers.[114] To ensure the balance between absorption and reflection, conductive and magnetic fillers are added in different layers, which leads to magnetoelectric synergy for EMI shielding. Thus, the asymmetric multilayered composites could realize a satisfactory EMI SE_T and a significant reduction of *R*-value. Frustratingly, the weak bonding force between layers can easily lead to the delamination of multilayered EMI shielding composites. Therefore, improving the interface bonding ability will be the focus of research for asymmetric multi-layered material.

(2) Asymmetric EMI shielding composites with fibrous structures have a three-dimensional framework that promotes electronic conduction and attenuation of EMWs. Asymmetric fibrous structures commonly consisting of a fibrous absorptive layer and a dense reflective layer contribute to the "absorption-reflection-reabsorption" shielding mechanism. Asymmetric EMI shielding fabrics hold the advantages of superior flexibility, tensile strength, and adjustable EMI shielding properties, which have set the stage for making their mark in EMI shielding fields. However, the challenges such as simplifying the preparation process and reducing cost need to be worked out in the future.

(3) Asymmetric EMI shielding composites with porous structures provide ultralightweight and durable peculiarity as well as the absorption-dominated EMI shielding property, which is favored in the military and aerospace fields.[115] To obtain satisfactory EMI SE_T, a highly conductive reflection layer at the transmitting surface is desirable to reflect EMWs back into the porous absorption layer.[116] Thus, such a designed structure extends the propagation path of the EMWs and increases the absorption and dissipation into heat against EMWs. However, asymmetric EMI foams sacrifice the thinness to achieve fascinating EMI shielding properties.[117]

(4) Asymmetric EMI shielding composites with segregated structures have the advantages of small filler addition and low cost.[118] A segregated structural layer combined with the compact reflective layer can remarkably reduce the escape of the EMWs, which reveals the superiority of the asymmetric segregated EMI shielding composites.[119] However, the weakened mechanical properties of asymmetric segregated composites are the main defects to limit their development.

Asymmetric EMI shielding composites exhibit scalable values in terms of structures and performances as well as applications.[120] With the deepening and development of research, it is expected that the design of asymmetric structures and novel nanofillers will breathe new life into outstanding EMI shielding materials.

BIOGRAPHIES

Lan Xie is a professor and the group leader of Material Big data and functional materials at Guizhou University. She received her Ph.D. from Sichuan University. At present, she has published more than 60 papers in international TOP journals such as Nano-Micro Letters. She has presided over more than 10 projects such as the National Natural Science Foundation and key basic projects of Guizhou Province. Her research focuses on big data technology, artificial intelligence, material big data and functional materials research.

Qiang Zheng is a professor and doctoral supervisor at Zhejiang University. He is a special professor of the "Changjiang Scholars Award Program" of the Ministry of Education, winner of the National Outstanding Young People Science Fund, and an expert enjoying special government subsidies. He presided over more than 40 projects such as the national key basic research and development plan (973 Plan). More than 640 academic papers have been included in SCI. His research focuses on polymer rheology, structure and properties of multi-component polymer materials, and the study of polymer composites.

Conflict of Interests

The authors declare no interest conflict.

ACKNOWLEDGMENTS

This work was financially supported by the National Natural Science Foundation of China (Nos. 52363004, 51963003 and 52263003), Guizhou Provincial Science and Technology Projects (Nos. ZK [2022] Maj019 and ZK [2023]-Nor160), and Guizhou Province High-level Innovative Talent Selection and Training Program (No. GCC2022-046).

REFERENCES

1 Zhang, Y.; Gu, J. A perspective for developing polymer-based electromagnetic interference shielding composites. *Nano-Micro Lett.* **2022**, *14*, 89.
2 Choi, Y. S.; Yoo, Y. H.; Kim, J. G.; Kim, S. H. A comparison of the corrosion resistance of Cu-Ni-stainless steel multilayers used for EMI shielding. *Surf. Coat. Tech.* **2006**, *201*, 3775–3782.
3 Zhang, C.; Li, Y.; Kang, W.; Liu, X.; Wang, Q. Current advances and future perspectives of additive manufacturing for functional polymeric materials and devices. *SusMat* **2021**, *1*, 127–147.
4 Geetha, S.; Satheesh, K. K. K.; Rao, C. R. K.; Vijayan, M.; Trivedi, D. C. EMI shielding: methods and materials—a review. *J. Appl. Polym. Sci.* **2009**, *112*, 2073–2086.
5 Liang, C.; Song, P.; Qiu, H.; Huang, F. Y.; Lu, Y.; Wang, L.; Kong, J.; Gu, J. Superior electromagnetic interference shielding performances of epoxy composites by introducing highly aligned reduced graphene oxide films. *Compos. Part A: Appl. S.* **2019**, *124*, 105512.
6 Liang, C.; Qiu, H.; Zhang, Y.; Liu, Y.; Gu, J. External field-assisted techniques for polymer matrix composites with electromagnetic interference shielding. *Sci. Bull.* **2023**, *68*, 1938–1953.
7 Song, W. L.; Cao, M. S.; Lu, M. M.; Bi, S.; Wang, C. Y.; Liu, J.; Yuan, J.; Fan, L. Z. Flexible graphene/polymer composite films in sandwich structures for effective electromagnetic interference shielding. *Carbon* **2014**, *66*, 67–76.
8 Onar, N.; Akşit, A. C.; Ebeoglugil, M. F.; Birlik, I.; Celik, E.; Ozdemir, I. Structural, electrical, and electromagnetic properties of cotton

fabrics coated with polyaniline and polypyrrole. *J. Appl. Polym. Sci.* **2009**, *114*, 2003–2010.
9 Chen, Y. H.; Huang, C. Y.; Roan, M. L.; Lai, F. D.; Chen, K. N.; Yeh, J. T. The copper sulfide coating on polyacrylonitrile with a chelating agent of ethylenediaminetetraacetic acid by an electroless deposition method and its EMI shielding effectiveness. *J. Appl. Polym. Sci.* **2010**, *115*, 570–578.
10 Sun, R.; Zhang, H. B.; Liu, J.; Xie, X.; Yang, R.; Li, Y.; Hong, S.; Yu, Z. Z. Highly conductive transition metal carbide/carbonitride (MXene)@polystyrene nanocomposites fabricated by electrostatic assembly for highly efficient electromagnetic interference shielding. *Adv. Funct. Mater.* **2017**, *27*, 1702807.
11 Li, Z.; Li, X.; Zong, Y.; Tan, G.; Sun, Y.; Lan, Y.; He, M.; Ren, Z.; Zheng, X. Solvothermal synthesis of nitrogen-doped graphene decorated by superparamagnetic Fe_3O_4 nanoparticles and their applications as enhanced synergistic microwave absorbers. *Carbon* **2017**, *115*, 493–502.
12 Sankaran, S.; Deshmukh, K.; Ahamed, M. B.; Khadheer, P. S. K. Recent advances in electromagnetic interference shielding properties of metal and carbon filler reinforced flexible polymer composites: a review. *Compos. Part A: Appl. S* **2018**, *114*, 49–71.
13 Wang, Y.; Gao, X.; Wu, X.; Luo, C. Facile synthesis of Mn_3O_4 hollow polyhedron wrapped by multiwalled carbon nanotubes as a high-efficiency microwave absorber. *Ceram. Int.* **2020**, *46*, 1560–1568.
14 Jiang, D.; Murugadoss, V.; Wang, Y.; Lin, J.; Ding, T.; Wang, Z.; Shao, Q.; Wang, C.; Liu, H.; Lu, N.; Wei, R.; Subramania, A.; Guo, Z. Electromagnetic interference shielding polymers and nanocomposites—a review. *Polym. Rev.* **2019**, *59*, 280–337.
15 Han, Y.; Ruan, K.; Gu, J. Janus (BNNS/ANF)-(AgNWs/ANF) thermal conductivity composite films with superior electromagnetic interference shielding and Joule heating performances. *Nano Res.* **2022**, *15*, 4747–4755.
16 Zhou, H.; Deng, H.; Zhang, L.; Wu, Z.; Deng, S.; Yang, W.; Zhang, Q.; Chen, F.; Fu, Q. Toward multi-functional polymer composites through selectively distributing functional fillers. *Compos. Part A: Appl. S* **2016**, *82*, 20–33.
17 Wen, C.; Zhao, B.; Liu, Y.; Xu, C.; Wu, Y.; Cheng, Y.; Liu, J.; Liu, Y.; Yang, Y.; Pan, H.; Zhang, J.; Wu, L.; Che, R. Flexible MXene-based composite films for multi-spectra defense in radar, infrared and visible light bands. *Adv. Funct. Mater.* **2023**, *33*, 2214223.
18 Sambyal, P.; Iqbal, A.; Hong, J.; Kim, M. K.; Kim, I. D.; Koo, C. M. Conductive MXene composites with liquid metal for high-performance electromagnetic interference shielding. *Mater. Chem. Phys.* **2023**, *295*, 127184.
19 Wang, W. Y.; Ma, X.; Shao, Y. W.; Qi, X. D.; Yang, J. H.; Wang, Y. Flexible, multifunctional, and thermally conductive nylon/graphene nanoplatelet composite papers with excellent EMI shielding performance, improved hydrophobicity and flame resistance. *J. Mater. Chem. A* **2021**, *9*, 5033–5044.
20 Wang, M.; Tang, X. H.; Cai, J. H.; Wu, H.; Shen, J. B.; Guo, S. Y. Construction, mechanism and prospective of conductive polymer composites with multiple interfaces for electromagnetic interference shielding: a review. *Carbon* **2021**, *177*, 377–402.
21 Li, N.; Huang, G. W.; Li, Y. Q.; Xiao, H. M.; Feng, Q. P.; Hu, N.; Fu, S. Y. Enhanced microwave absorption performance of coated carbon nanotubes by optimizing the Fe_3O_4 nanocoating structure. *ACS Appl. Mater. Interfaces* **2017**, *9*, 2973–2983.
22 Zeng, S.; Li, X.; Li, M.; Zheng, J.; E, S.; Yang, W.; Zhao, B.; Guo, X.; Zhang, R. Flexible PVDF/CNTs/Ni@CNTs composite films possessing excellent electromagnetic interference shielding and mechanical properties under heat treatment. *Carbon* **2019**, *155*, 34–43.
23 Liang, C.; Song, P.; Qiu, H.; Zhang, Y.; Ma, X.; Qi, F.; Gu, H.; Kong, J.; Cao, D.; Gu, J. Constructing interconnected spherical hollow conductive networks in silver platelets/reduced graphene oxide foam/epoxy nanocomposites for superior electromagnetic interference shielding effectiveness. *Nanoscale* **2019**, *11*, 22590–22598.
24 Li, X. H.; Li, X.; Liao, K. N.; Min, P.; Liu, T.; Dasari, A.; Yu, Z. Z. Thermally annealed anisotropic graphene aerogels and their electrically conductive epoxy composites with excellent electromagnetic interference shielding efficiencies. *ACS Appl. Mater. Interfaces* **2016**, *8*, 33230–33239.
25 Al-Saleh, M. H.; Saadeh, W. H.; Sundararaj, U. EMI shielding effectiveness of carbon based nanostructured polymeric materials: a comparative study. *Carbon* **2013**, *60*, 146–156.
26 Gu, J.; Ruan, K. Breaking through bottlenecks for thermally conductive polymer composites: a perspective for intrinsic thermal conductivity, interfacial thermal resistance and theoretics. *Nanomicro Lett.* **2021**, *13*, 110.
27 Li, W.; Li, X.; Chang, W.; Wu, J.; Liu, P.; Wang, J.; Yao, X.; Yu, Z. Z. Vertically aligned reduced graphene oxide/$Ti_3C_2T_x$ MXene hybrid hydrogel for highly efficient solar steam generation. *Nano Res.* **2020**, *13*, 3048–3056.
28 Yin, D.; Pan, Y.; Guo, Q.; Wang, Y.; Huang, J. Preparation and properties of flexible nanocellulose fibers/Ag nanoparticles composite films with excellent electromagnetic shielding performance. *Appl. Phys. A-Mater.* **2021**, *128*, 43.
29 Sorgucu, U. Enhancing the electromagnetic shielding effectiveness of alumina (Al_2O_4) by coating with nano gold (AuNp). *Opt. Mater.* **2024**, *148*, 114795.
30 Gu, T.; Zeng, Z.; Wu, S.; Sun, D. X.; Zhao, C. S.; Wang, Y. Poly(L-lactic acid)/graphene composite films with asymmetric sandwich structure for thermal management and electromagnetic interference shielding. *Chem. Eng. J.* **2023**, *466*, 143190.
31 Lu, X.; Zheng, Y.; Yang, J.; Qu, J. Multifunctional paraffin wax/carbon nanotube sponge composites with simultaneous high-efficient thermal management and electromagnetic interference shielding efficiencies for electronic devices. *Compos. Part B: Eng.* **2020**, *199*, 108308.
32 Wang, L.; Chen, L.; Song, P.; Liang, C.; Lu, Y.; Qiu, H.; Zhang, Y.; Kong, J.; Gu, J. Fabrication on the annealed $Ti_3C_2T_x$ MXene/epoxy nanocomposites for electromagnetic interference shielding application. *Compos. Part B: Eng.* **2019**, *171*, 111–118.
33 Qin, F.; Brosseau, C. A review and analysis of microwave absorption in polymer composites filled with carbonaceous particles. *J. Appl. Phys.* **2012**, *111*.
34 Wu, T.; Liu, Y.; Zeng, X.; Cui, T.; Zhao, Y.; Li, Y.; Tong, G. Facile hydrothermal synthesis of Fe_3O_4/C core-shell nanorings for efficient low-frequency microwave absorption. *ACS Appl. Mater. Interfaces* **2016**, *8*, 7370–7380.
35 González, M.; Pozuelo, J.; Baselga, J. Electromagnetic shielding materials in GHz range. *Chem. Rec.* **2018**, *18*, 1000–1009.
36 Singh, A. K.; Shishkin, A.; Koppel, T.; Gupta, N. A review of porous lightweight composite materials for electromagnetic interference shielding. *Compos. Part B: Eng.* **2018**, *149*, 188–197.
37 Yang, S.; Yang, P.; Ren, C.; Zhao, X.; Zhang, J. Millefeuille-inspired highly conducting polymer nanocomposites based on controllable layer-by-layer assembly strategy for durable and stable electromagnetic interference shielding. *J. Colloid. Interf. Sci.* **2022**, *622*, 97–108.
38 Li, L.; Ma, Z.; Xu, P.; Zhou, B.; Li, Q.; Ma, J.; He, C.; Feng, Y.; Liu, C. Flexible and alternant-layered cellulose nanofiber/graphene film with superior thermal conductivity and efficient electromagnetic interference shielding. *Compos. Part A: Appl. S* **2020**, *139*, 106134.

https://doi.org/10.1007/s10118-024-3112-x

39 He, W.; Chen, G.; Li, C.; Chen, X.; Chen, Y.; Xiong, M.; Niu, X.; Zhu, M.; Li, X. Magnetically aligned CNT/magnetite heterogeneous composite membranes for electromagnetic wave shielding and heat dissipation. *Mater. Res. Bull.* **2022**, *149*, 111748.

40 Tao, Q.; Men, C.; Li, C.; Cong, S.; Hu, D.; Li, Q. A Janus-structured Fe_3O_4-PDMS/CNT/Cu composite film for extreme-environmental electromagnetic interference shielding. *Mater. Lett.* **2022**, *326*, 132892.

41 Hu, G.; Wu, C.; Wang, Q.; Dong, F.; Xiong, Y. Ultrathin nanocomposite films with asymmetric gradient alternating multilayer structures exhibit superhigh electromagnetic interference shielding performances and robust mechanical properties. *Chem. Eng. J.* **2022**, *447*, 137537.

42 Xu, Y.; Yang, Y.; Yan, D. X.; Duan, H.; Zhao, G.; Liu, Y. Gradient structure design of flexible waterborne polyurethane conductive films for ultraefficient electromagnetic shielding with low reflection characteristic. *ACS Appl. Mater. Interfaces* **2018**, *10*, 19143–19152.

43 Sheng, A.; Ren, W.; Yang, Y.; Yan, D. X.; Duan, H.; Zhao, G.; Liu, Y.; Li, Z. M. Multilayer WPU conductive composites with controllable electro-magnetic gradient for absorption-dominated electromagnetic interference shielding. *Compos. Part A: Appl. S* **2020**, *129*, 105692.

44 Zhou, B.; Li, Q.; Xu, P.; Feng, Y.; Ma, J.; Liu, C.; Shen, C. An asymmetric sandwich structural cellulose-based film with self-supported MXene and AgNW layers for flexible electromagnetic interference shielding and thermal management. *Nanoscale* **2021**, *13*, 2378–2388.

45 Zhang, F.; Ren, P.; Guo, Z.; Wang, J.; Chen, Z.; Zong, Z.; Hu, J.; Jin, Y.; Ren, F. Asymmetric multilayered MXene-AgNWs/cellulose nanofiber composite films with antibacterial properties for high-efficiency electromagnetic interference shielding. *J. Mater. Sci. Technol.* **2022**, *129*, 181–189.

46 Guo, Z.; Ren, P.; Lu, Z.; Hui, K.; Yang, J.; Zhang, Z.; Chen, Z.; Jin, Y.; Ren, F. Multifunctional $CoFe_2O_4$@MXene-AgNWs/cellulose nanofiber composite films with asymmetric layered architecture for high-efficiency electromagnetic interference shielding and remarkable thermal management capability. *ACS Appl. Mater. Interfaces* **2022**, *14*, 41468–41480.

47 Cao, W.; Ma, C.; Tan, S.; Ma, M.; Wan, P.; Chen, F. Ultrathin and flexible CNTs/MXene/cellulose nanofibrils composite paper for electromagnetic interference shielding. *Nanomicro Lett.* **2019**, *11*, 72.

48 Lai, Z.; Cheng, K.; Zhao, T.; Zhu, P.; Liu, D.; Liang, X.; Sun, R. A facile process to fabricate copper/nickel-coated polyurethane composite with high electromagnetic interference shielding performance. *Compos. Commun.* **2023**, *38*, 101487.

49 Yuan, M.; Fei, Y.; Zhang, H.; Qiu, B.; Shen, L.; He, X.; Liang, M.; Zhou, S.; Chen, Y.; Zou, H. Electromagnetic asymmetric films comprise metal organic frameworks derived porous carbon for absorption-dominated electromagnetic interference shielding. *Compos. Part B: Eng.* **2022**, *233*, 109622.

50 Mai, T.; Guo, W. Y.; Wang, P. L.; Chen, L.; Qi, M. Y.; Liu, Q.; Ding, Y.; Ma, M. G. Bilayer metal-organic frameworks/MXene/nanocellulose paper with electromagnetic double loss for absorption-dominated electromagnetic interference shielding. *Chem. Eng. J.* **2023**, *464*, 142517.

51 Breuer, O.; Sundararaj, U. Big returns from small fibers: a review of polymer/carbon nanotube composites. *Polym. Compos.* **2004**, *25*, 630–645.

52 Gong, S.; Zhu, Z. H.; Meguid, S. A. Carbon nanotube agglomeration effect on piezoresistivity of polymer nanocomposites. *Polymer* **2014**, *55*, 5488–5499.

53 Gong, S.; Zhu, Z. H.; Li, J.; Meguid, S. A. Modeling and characterization of carbon nanotube agglomeration effect on electrical conductivity of carbon nanotube polymer composites. *J. Appl. Phys.* **2014**, *116*, 194306.

54 Chen, Y.; Zhang, H. B.; Yang, Y.; Wang, M.; Cao, A.; Yu, Z. Z. High-performance epoxy nanocomposites reinforced with three-dimensional carbon nanotube sponge for electromagnetic interference shielding. *Adv. Funct. Mater.* **2016**, *26*, 447–455.

55 He, Q. M.; Tao, J. R.; Yang, Y.; Yang, D.; Zhang, K.; Fei, B.; Wang, M. Electric-magnetic-dielectric synergism and Salisbury screen effect in laminated polymer composites with multiwall carbon nanotube, nickel, and antimony trioxide for enhancing electromagnetic interference shielding. *Compos. Part A: Appl. S.* **2022**, *156*, 106901.

56 Balandin, A. A.; Ghosh, S.; Bao, W.; Calizo, I.; Teweldebrhan, D.; Miao, F.; Lau, C. N. Superior thermal conductivity of single-layer graphene. *Nano Lett.* **2008**, *8*, 902–907.

57 Novoselov, K. S.; Geim, A. K.; Morozov, S. V.; Jiang, D.; Zhang, Y.; Dubonos, S. V.; Grigorieva, I. V.; Firsov, A. A. Electric field effect in atomically thin carbon films. *Science* **2004**, *306*, 666–669.

58 Novoselov, K. S.; Geim, A. K.; Morozov, S. V.; Jiang, D.; Katsnelson, M. I.; Grigorieva, I. V.; Dubonos, S. V.; Firsov, A. A. Two-dimensional gas of massless Dirac fermions in graphene. *Nature* **2005**, *438*, 197–200.

59 Lin, J. H.; Lin, Z. I.; Pan, Y. J.; Huang, C. L.; Chen, C. K.; Lou, C. W. Polymer composites made of multi-walled carbon nanotubes and graphene nano-sheets: Effects of sandwich structures on their electromagnetic interference shielding effectiveness. *Compos. Part B: Eng.* **2016**, *89*, 424–431.

60 Sefadi, J. S.; Luyt, A. S.; Pionteck, J.; Piana, F.; Gohs, U. Effect of surfactant and electron treatment on the electrical and thermal conductivity as well as thermal and mechanical properties of ethylene vinyl acetate/expanded graphite composites. *J. Appl. Polym. Sci.* **2015**, *132*, 42396.

61 Konkena, B.; Vasudevan, S. Understanding aqueous dispersibility of graphene oxide and reduced graphene oxide through pK_a measurements. *J. Phys. Chem. Lett.* **2012**, *3*, 867–872.

62 Zhang, Y.; Ruan, K.; Zhou, K.; Gu, J. Controlled distributed $Ti_3C_2T_x$ hollow microspheres on thermally conductive polyimide composite films for excellent electromagnetic interference shielding. *Adv. Mater.* **2023**, *35*, 2211642.

63 Wang, J.; Song, T.; Ming, W.; Yele, M.; Chen, L.; Zhang, H.; Zhang, X.; Liang, B.; Wang, G. High MXene loading, nacre-inspired MXene/ANF electromagnetic interference shielding composite films with ultralong strain-to-failure and excellent Joule heating performance. *Nano Res.* **2024**, *17*, 2061–2069.

64 Gong, S.; Sheng, X.; Li, X.; Sheng, M.; Wu, H.; Lu, X.; Qu, J. A multifunctional flexible composite film with excellent multi-source driven thermal management, electromagnetic interference shielding, and fire safety performance, inspired by a "brick-mortar" sandwich structure. *Adv. Funct. Mater.* **2022**, *32*, 2200570.

65 Li, M.; Sun, Y.; Feng, D.; Ruan, K.; Liu, X.; Gu, J. Thermally conductive polyvinyl alcohol composite films *via* introducing hetero-structured MXene@silver fillers. *Nano Res.* **2023**, *16*, 7820–7828.

66 Maleski, K.; Mochalin, V. N.; Gogotsi, Y. Dispersions of two-dimensional titanium carbide MXene in organic solvents. *Chem. Mater.* **2017**, *29*, 1632–1640.

67 Velusamy, D. B.; Kim, R. H.; Cha, S.; Huh, J.; Khazaeinezhad, R.; Kassani, S. H.; Song, G.; Cho, S. M.; Cho, S. H.; Hwang, I.; Lee, J.; Oh, K.; Choi, H.; Park, C. Flexible transition metal dichalcogenide nanosheets for band-selective photodetection. *Nat. Commun.* **2015**, *6*, 8063.

68 Sundaram, H. S.; Han, X.; Nowinski, A. K.; Ella-Menye, J. R.; Wimbish, C.; Marek, P.; Senecal, K.; Jiang, S. One-step dip

coating of zwitterionic sulfobetaine polymers on hydrophobic and hydrophilic surfaces. *ACS Appl. Mater. Interfaces* **2014**, *6*, 6664–6671.
69 Carey, T.; Jones, C.; Le Moal, F.; Deganello, D.; Torrisi, F. Spray-coating thin films on three-dimensional surfaces for a semitransparent capacitive-touch device. *ACS Appl. Mater. Interfaces* **2018**, *10*, 19948–19956.
70 Jo, J. W.; Jung, J. W.; Lee, J. U.; Jo, W. H. Fabrication of highly conductive and transparent thin films from single-walled carbon nanotubes using a new non-ionic surfactant *via* spin coating. *ACS Nano* **2010**, *4*, 5382–5388.
71 Yun, T.; Kim, J. S.; Shim, J.; Choi, D. S.; Lee, K. E.; Koo, S. H.; Kim, I.; Jung, H. J.; Yoo, H. W.; Jung, H. T.; Kim, S. O. Ultrafast interfacial self-assembly of 2D transition metal dichalcogenides monolayer films and their vertical and in-plane heterostructures. *ACS Appl. Mater. Interfaces* **2017**, *9*, 1021–1028.
72 Zhang, Y.; Ruan, K.; Guo, Y.; Gu, J. Recent advances of MXenes-based optical functional materials. *Adv. Photon. Res.* **2023**, *4*, 2300224.
73 Liu, Q.; Zhang, Y.; Liu, Y.; Li, C.; Liu, Z.; Zhang, B.; Zhang, Q. Magnetic field-induced strategy for synergistic CI/$Ti_3C_2T_x$/PVDF multilayer structured composite films with excellent electromagnetic interference shielding performance. *J. Mater. Sci. Technol.* **2022**, *110*, 246–259.
74 Wang, Y.; Zhang, W.; Wu, X.; Luo, C.; Liang, T.; Yan, G. Metal-organic framework nanoparticles decorated with graphene: a high-performance electromagnetic wave absorber. *J. Magn. Magn. Mater.* **2016**, *416*, 226–230.
75 Yang, D.; Zhang, C.; Biendicho, J. J.; Han, X.; Liang, Z.; Du, R.; Li, M.; Li, J.; Arbiol, J.; Llorca, J.; Zhou, Y.; Morante, J. R.; Cabot, A. ZnSe/N-doped carbon nanoreactor with multiple adsorption sites for stable lithium-sulfur batteries. *ACS Nano* **2020**, *14*, 15492–15504.
76 Zhang, Y.; Yang, S.; Zhang, Q.; Ma, Z.; Guo, Y.; Shi, M.; Wu, H.; Guo, S. Constructing interconnected asymmetric conductive network in TPU fibrous film: achieving low-reflection electromagnetic interference shielding and surperior thermal conductivity. *Carbon* **2023**, *206*, 37–44.
77 Zhang, Y.; Ma, Z.; Ruan, K.; Gu, J. Flexible $Ti_3C_2T_x$/(aramid nanofiber/PVA) composite films for superior electromagnetic interference shielding. *Research* **2022**, *2022*, 9780290.
78 Yang, M.; Jia, X.; He, D.; Ma, Y.; Cheng, Y.; Wang, J.; Li, Y.; Wang, C. Superhydrophobic and corrosion-resistant electrospun hybrid membrane for high-efficiency electromagnetic interference shielding. *ACS Appl. Electron. Mater.* **2021**, *3*, 2067–2078.
79 Cui, C.; Xiang, C.; Geng, L.; Lai, X.; Guo, R.; Zhang, Y.; Xiao, H.; Lan, J.; Lin, S.; Jiang, S. Flexible and ultrathin electrospun regenerate cellulose nanofibers and d-$Ti_3C_2T_x$ (MXene) composite film for electromagnetic interference shielding. *J. Alloy. Compd.* **2019**, *788*, 1246–1255.
80 Kim, M.; Kim, S.; Seong, Y. C.; Yang, K. H.; Choi, H. Multiwalled carbon nanotube buckypaper/polyacrylonitrile nanofiber composite membranes for electromagnetic interference shielding. *ACS Appl. Nano Mater.* **2021**, *4*, 729–738.
81 Zhang, S.; Huang, X.; Xiao, W.; Zhang, L.; Yao, H.; Wang, L.; Luo, J.; Gao, J. Polyvinylpyrrolidone assisted preparation of highly conductive, antioxidation, and durable nanofiber composite with an extremely high electromagnetic interference shielding effectiveness. *ACS Appl. Mater. Interfaces* **2021**, *13*, 21865–21875.
82 Zhang, N.; Zhao, R.; He, D.; Ma, Y.; Qiu, J.; Jin, C.; Wang, C. Lightweight and flexible Ni-Co alloy nanoparticle-coated electrospun polymer nanofiber hybrid membranes for high-performance electromagnetic interference shielding. *J. Alloy. Compd.* **2019**, *784*, 244–255.
83 Lee, S.; Park, J.; Kim, M. C.; Kim, M.; Park, P.; Yoon, I. J.; Nah, J. Polyvinylidene fluoride core-shell nanofiber membranes with highly conductive shells for electromagnetic interference shielding. *ACS Appl. Mater. Interfaces* **2021**, *13*, 25428–25437.
84 Guo, Y.; Qiu, H.; Ruan, K.; Wang, S.; Zhang, Y.; Gu, J. Flexible and insulating silicone rubber composites with sandwich structure for thermal management and electromagnetic interference shielding. *Compos. Sci. Technol.* **2022**, *219*, 109253.
85 Deng, H.; Skipa, T.; Bilotti, E.; Zhang, R.; Lellinger, D.; Mezzo, L.; Fu, Q.; Alig, I.; Peijs, T. Preparation of high-performance conductive polymer fibers through morphological control of networks formed by nanofillers. *Adv. Funct. Mater.* **2010**, *20*, 1424–1432.
86 Lv, Z.; Kong, L.; Sun, P.; Lin, Y.; Wang, Y.; Xiao, C.; Liu, X.; Zhang, X.; Zheng, K.; Tian, X. Dual-functional eco-friendly liquid metal/boron nitride/silk fibroin composite film with outstanding thermal conductivity and electromagnetic shielding efficiency. *Compos. Commun.* **2023**, *39*, 101565.
87 Jia, L.; Ding, X.; Sun, J.; Zhang, X.; Tian, X. A controllable gradient structure of hydrophobic composite fabric constructed by silver nanowires and polyvinylidene fluoride microspheres for electromagnetic interference shielding with low reflection. *Compos. Part A: Appl. S* **2022**, *156*, 106884.
88 Xiao, W.; Zhang, L.; Zhang, S.; Yan, J.; Zhang, G.; Gao, J. Electrically conductive and magnetic nanofiber composites with an asymmetric structure for efficient electromagnetic interference shielding. *Colloid. Surf. A* **2023**, *675*, 132063.
89 Zhang, X.; Tang, J.; Zhong, Y.; Feng, Y.; Wei, X.; Li, M.; Wang, J. Asymmetric layered structural design with metal microtube conductive network for absorption-dominated electromagnetic interference shielding. *Colloid. Surf. A* **2022**, *643*, 128781.
90 Chen, T.; Cai, J.; Cheng, X.; Cui, S.; Zhang, D.; Gong, D. Bio-inspired flexible versatile textiles for excellent absorption-dominated electromagnetic interference shielding, thermal management, and strain sensing. *Chem. Eng. J.* **2023**, *477*, 147116.
91 Xue, B.; Li, Y.; Cheng, Z.; Yang, S.; Xie, L.; Qin, S.; Zheng, Q. Directional electromagnetic interference shielding based on step-wise asymmetric conductive networks. *Nanomicro Lett.* **2021**, *14*, 16.
92 Zhang, J.; Zhu, D.; Zhang, S.; Cheng, H.; Chen, S.; Tang, R.; Hang, Z. H.; Zhang, T.; Zhang, X.; Yang, Z. Asymmetric electromagnetic shielding performance based on spatially controlled deposition of nickel nanoparticles on carbon nanotube sponge. *Carbon* **2022**, *194*, 290–296.
93 Yang, J.; Liao, X.; Wang, G.; Chen, J.; Guo, F.; Tang, W.; Wang, W.; Yan, Z.; Li, G. Gradient structure design of lightweight and flexible silicone rubber nanocomposite foam for efficient electromagnetic interference shielding. *Chem. Eng. J.* **2020**, *390*, 124589.
94 Yang, J.; Liao, X.; Wang, G.; Chen, J.; Song, P.; Tang, W.; Guo, F.; Liu, F.; Li, G. Heterogeneous silicon rubber composite foam with gradient porous structure for highly absorbed ultra-efficient electromagnetic interference shielding. *Compos. Sci. Technol.* **2021**, *206*, 108663.
95 Lei, Z.; Tian, D.; Liu, X.; Wei, J.; Rajavel, K.; Zhao, T.; Hu, Y.; Zhu, P.; Sun, R.; Wong, C. P. Electrically conductive gradient structure design of thermoplastic polyurethane composite foams for efficient electromagnetic interference shielding and ultra-low microwave reflectivity. *Chem. Eng. J.* **2021**, *424*, 130365.
96 Duan, H.; Zhu, H.; Gao, J.; Yan, D. X.; Dai, K.; Yang, Y.; Zhao, G.; Liu, Y.; Li, Z. M. Asymmetric conductive polymer composite foam for absorption dominated ultra-efficient electromagnetic interference shielding with extremely low reflection

characteristics. *J. Mater. Chem. A* **2020**, *8*, 9146–9159.
97 Gao, Q.; Zhang, G.; Zhang, Y.; Fan, X.; Wang, Z.; Zhang, S.; Xiao, R.; Huang, F.; Shi, X.; Qin, J. Absorption dominated high-performance electromagnetic interference shielding epoxy/functionalized reduced graphene oxide/Ni-chains microcellular foam with asymmetric conductive structure. *Compos. Sci. Technol.* **2022**, *223*, 109419.
98 Li, M.; Feng, Y.; Wang, J. Asymmetric conductive structure design for stabilized composites with absorption dominated ultra-efficient electromagnetic interference shielding performance. *Compos. Sci. Technol.* **2023**, *236*, 110006.
99 Liu, G.; Yu, R.; Liu, D.; Xia, Y.; Pei, X.; Wang, W.; Min, C.; Liu, S.; Shao, R.; Xu, Z. 3D-printed TiO_2-$Ti_3C_2T_x$ heterojunction/rGO/PDMS composites with gradient pore size for electromagnetic interference shielding and thermal management. *Compos. Part A: Appl. S*. **2022**, *160*, 107058.
100 Zuo, T.; Xie, C.; Wang, W.; Yu, D. $Ti_3C_2T_x$ MXene-ferroferric oxide/carbon nanotubes/waterborne polyurethane-based asymmetric composite aerogels for absorption-dominated electromagnetic interference shielding. *ACS Appl. Nano Mater.* **2023**, *6*, 4716–4725.
101 Pei, X.; Liu, G.; Shi, H.; Yu, R.; Wang, S.; Liu, S.; Min, C.; Song, J.; Shao, R.; Xu, Z. Directional electromagnetic interference shielding of asymmetric structure based on dual-needle 3D printing. *Compos. Sci. Technol.* **2023**, *233*, 109909.
102 Yao, J.; Zhou, J.; Yang, F.; Peng, G.; Liu, Y.; Yao, Z.; Wu, F.; Zeng, H. Multi-functional and multi-scenario applications for MXene aerogels with synergistically enhanced asymmetric modules. *Nano Res.* **2024**, *17*, 3359–3368.
103 Zuo, T.; Wang, W.; Yu, D. MXene/Ag@ZnO/WPU/Melamine gradient composite foams prepared by a unidirectional evaporation approach for absorption-dominated electromagnetic interference shielding. *J. Alloy. Compd.* **2023**, *966*, 171644.
104 Zhang, Y. P.; Zhou, C. G.; Sun, W. J.; Wang, T.; Jia, L. C.; Yan, D. X.; Li, Z. M. Injection molding of segregated carbon nanotube/polypropylene composite with enhanced electromagnetic interference shielding and mechanical performance. *Compos. Sci. Technol.* **2020**, *197*, 108253.
105 Jia, L. C.; Jia, X. X.; Sun, W. J.; Zhang, Y. P.; Xu, L.; Yan, D. X.; Su, H. J.; Li, Z. M. Stretchable liquid metal-based conductive textile for electromagnetic interference shielding. *ACS Appl. Mater. Interfaces* **2020**, *12*, 53230–53238.
106 Li, Y.; Tian, X.; Gao, S. P.; Jing, L.; Li, K.; Yang, H.; Fu, F.; Lee, J. Y.; Guo, Y. X.; Ho, J. S.; Chen, P. Y. Reversible crumpling of 2D titanium carbide (MXene) nanocoatings for stretchable electromagnetic shielding and wearable wireless communication. *Adv. Funct. Mater.* **2020**, *30*, 1907451.
107 Zhan, Y.; Wang, J.; Zhang, K.; Li, Y.; Meng, Y.; Yan, N.; Wei, W.; Peng, F.; Xia, H. Fabrication of a flexible electromagnetic interference shielding Fe_3O_4@reduced graphene oxide/natural rubber composite with segregated network. *Chem. Eng. J.* **2018**, *344*, 184–193.
108 Yu, W. C.; Wang, T.; Liu, Y. H.; Wang, Z. G.; Xu, L.; Tang, J. H.; Dai, K.; Duan, H. J.; Xu, J. Z.; Li, Z. M. Superior and highly absorbed electromagnetic interference shielding performance achieved by designing the reflection-absorption-integrated shielding compartment with conductive wall and lossy core. *Chem. Eng. J.* **2020**, *393*, 124644.
109 Sun, B.; Sun, S.; He, P.; Mi, H. Y.; Dong, B.; Liu, C.; Shen, C. Asymmetric layered structural design with segregated conductive network for absorption-dominated high-performance electromagnetic interference shielding. *Chem. Eng. J.* **2021**, *416*, 129083.
110 Liu, F.; Wei, Z.; Hu, X.; Cai, Y.; Chen, Z.; Yang, C.; Zhan, Y.; Xia, H. Asymmetric segregated network design of ultralight and thermal insulating polymer composite foams for green electromagnetic interference shielding. *Compos. Commun.* **2023**, *38*, 101492.
111 Wang, Z.; Wang, S.; Zhang, K.; Shen, Z.; Yu, E.; Zheng, S. Y.; Liu, S.; Yang, J. Heterostructured composite foam with highly efficient absorption-dominant EMI shielding capability and mechanical robustness. *Compos. Commun.* **2023**, *40*, 101603.
112 Wu, B.; Liu, R.; Yang, Y.; Zhu, H.; Yu, Y.; Huang, J.; Li, Y. Asymmetrically structured polyvinylidene fluoride composite for directional high absorbed electromagnetic interference shielding. *J. Appl. Polym. Sci.* **2023**, *140*, 53340.
113 Liang, C.; Gu, Z.; Zhang, Y.; Ma, Z.; Qiu, H.; Gu, J. Structural design strategies of polymer matrix composites for electromagnetic interference shielding: a review. *Nano-Micro Lett.* **2021**, *13*, 181.
114 Ma, T. B.; Ma, H.; Ruan, K. P.; Shi, X. T.; Qiu, H.; Gao, S. Y.; Gu, J. W. Thermally conductive poly(lactic acid) composites with superior electromagnetic shielding performances *via* 3D printing technology. *Chinese J. Polym. Sci.* **2022**, *40*, 248–255.
115 Wang, Y. Y.; Zhou, Z. H.; Zhou, C. G.; Sun, W. J.; Gao, J. F.; Dai, K.; Yan, D. X.; Li, Z. M. Lightweight and robust carbon nanotube/polyimide foam for efficient and heat-resistant electromagnetic interference shielding and microwave absorption. *ACS Appl. Mater. Inter.* **2020**, *12*, 8704–8712.
116 Yang, J.; Wang, H.; Zhang, Y.; Zhang, H.; Gu, J. Layered structural PBAT composite foams for efficient electromagnetic interference shielding. *Nano-Micro Lett.* **2023**, *16*, 31.
117 Wang, L.; Ma, Z.; Zhang, Y.; Chen, L.; Cao, D.; Gu, J. Polymer-based EMI shielding composites with 3D conductive networks: a mini-review. *SusMat* **2021**, *1*, 413–431.
118 Wang, T.; Kong, W. W.; Yu, W. C.; Gao, J. F.; Dai, K.; Yan, D. X.; Li, Z. M. A healable and mechanically enhanced composite with segregated conductive network structure for high-efficient electromagnetic interference shielding. *Nano-Micro Lett.* **2021**, *13*, 162.
119 Yang, J.; Chen, Y.; Yan, X.; Liao, X.; Wang, H.; Liu, C.; Wu, H.; Zhou, Y.; Gao, H.; Xia, Y.; Zhang, H.; Li, X.; Wang, T. Construction of *in-situ* grid conductor skeleton and magnet core in biodegradable poly(butyleneadipate-*co*-terephthalate) for efficient electromagnetic interference shielding and low reflection. *Compos. Sci. Technol.* **2023**, *240*, 110093.
120 Gong, K.; Peng, Y.; Liu, A.; Qi, S.; Qiu, H. Ultrathin carbon layer coated MXene/PBO nanofiber films for excellent electromagnetic interference shielding and thermal stability. *Compos. Part A: Appl. S* **2024**, *176*, 107857.

https://doi.org/10.1007/s10118-024-3112-x